

# In Defense of the Unitary Scalarization for Deep Multi-Task Learning

Vitaly Kurin <sup>\*1</sup> Alessandro De Palma <sup>\*1</sup> Ilya Kostrikov <sup>2,3</sup> Shimon Whiteson <sup>1</sup> M. Pawan Kumar <sup>1</sup>

## Abstract

Recent multi-task learning research argues against *unitary scalarization*, where training simply minimizes the sum of the task losses. Several ad-hoc multi-task optimization algorithms have instead been proposed, inspired by various hypotheses about what makes multi-task settings difficult. The majority of these optimizers require per-task gradients, and introduce significant memory, runtime, and implementation overhead. We present a theoretical analysis suggesting that many specialized multi-task optimizers can be interpreted as forms of regularization. Moreover, we show that, when coupled with standard regularization and stabilization techniques from single-task learning, unitary scalarization matches or improves upon the performance of complex multi-task optimizers in both supervised and reinforcement learning settings. We believe our results call for a critical reevaluation of recent research in the area.

## 1. Introduction

Multi-Task Learning (MTL) (Caruana, 1997a) exploits similarities between tasks to yield models that are more accurate, generalize better and require less training data. Owing to the success of MTL on traditional machine learning models (Heskes, 2000; Bakker & Heskes, 2003; Evgeniou & Pontil, 2004) and of deep single-task learning across a variety of domains, a growing body of research has focused on deep MTL. The most straightforward way to train a neural network for multiple tasks at once is to minimize the sum of per-task losses. Adopting terminology from multi-objective optimization, we call this approach *unitary scalarization*.

While some work shows that multi-task networks trained via unitary scalarization exhibit superior performance to independent per-task models (Kokkinos, 2017; Kalashnikov et al., 2021), others suggest the opposite (Teh et al., 2017b;

<sup>\*</sup>Equal contribution <sup>1</sup>University of Oxford, United Kingdom <sup>2</sup>UC Berkeley, USA <sup>3</sup>work partly done at NYU, USA. Correspondence to: Vitaly Kurin <vitaly.kurin@cs.ox.ac.uk>, Alessandro De Palma <adepalma@robots.ox.ac.uk>.

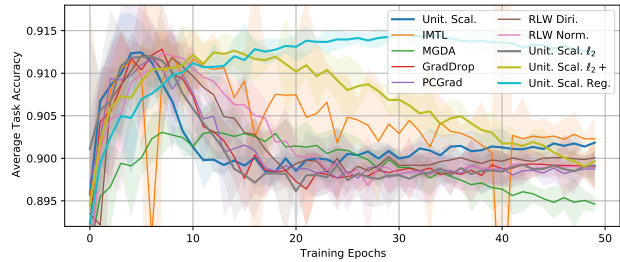


Figure 1. Mean and 95% CI (3 runs) avg. task validation accuracy per training epoch on CelebA (Liu et al., 2015). SMTOs postpone the onset of overfitting, closely matching the effect of  $\ell_2$  regularization on unitary scalarization. Two different  $\ell_2$  penalty terms are shown. The addition of dropout layers (“Reg.”) further reduces overfitting. See appendix C.2 for details.

Kendall et al., 2018; Sener & Koltun, 2018). As a result, many explanations for the difficulty of MTL have been proposed, each motivating a new Specialized Multi-Task Optimizer (SMTO) (Sener & Koltun, 2018; Liu et al., 2021; Yu et al., 2020; Chen et al., 2020; Wang et al., 2021). These works typically claim that the proposed SMTO outperforms unitary scalarization, in addition to relevant prior work. However, SMTOs usually require access to per-task gradients either with respect to the shared parameters, or to the shared representation. Therefore, their reported performance gain comes at significant computation and memory cost, the overhead scaling linearly with the number of tasks. By contrast, unitary scalarization requires only the average of the gradients across tasks, which can be computed via a single backpropagation.

Existing SMTOs were introduced to solve challenges related to the optimization of the deep MTL problem. We instead postulate that the reported weakness of unitary scalarization is linked to experimental variability or to a lack of regularization, leading to the following contributions:

- A theoretical analysis of popular SMTOs based on per-task gradients (§4), suggesting that all the considered methods reduce overfitting on the multi-task problem. In other words, we present novel technical results reinterpreting SMTOs as implicit regularizers. Figure 1 supports this empirically, showing that SMTOs behave similarly to a  $\ell_2$ -penalized unitary scalarization. Further evidence is presented in appendix C.2.

- A comprehensive experimental evaluation (§5) of recent SMTOS on popular multi-task benchmarks, showing that no SMTO consistently outperforms unitary scalarization in spite of the added complexity and overhead. In particular, either the differences between unitary scalarization and SMTOS are not statistically significant, or they can be bridged by standard regularization and stabilization techniques from the single-task literature. Our reinforcement learning (RL) experiments include methods previously considered only on supervised learning.

We believe that our technical (§4) and empirical (§5) results suggest that the considered SMTOS can be replaced by less expensive and well-established techniques. We hope that these surprising results stimulate the search for a deeper understanding of the area.

## 2. Related Work

Before diving into details of specific SMTOS in Section 4, we provide a high-level overview of the deep MTL research. MTL is represented by a vast body of literature, including Caruana’s pioneering work (Caruana, 1997b) exploring *hard parameter sharing*, i.e., sharing neural network parameters between all tasks with, possibly, a separate part of the model for each task. Hard parameter sharing is still the major MTL approach adopted in natural language processing (Collobert & Weston, 2008; Chen et al., 2021), computer vision (Misra et al., 2016), and speech recognition (Seltzer & Droppo, 2013). In this work, we implicitly assume that each parameter update employs information from all tasks. However, not all works satisfy this assumption, either due to a large number of tasks (Cappart et al., 2021; Kurin et al., 2020), or, simply, as an implementation decision (Huang et al., 2020; Kurin et al., 2021). In this setting, MTL resembles other problems dealing with multiple tasks, i.e., continual (Khetarpal et al., 2020), curriculum (Narvekar et al., 2020), and meta-learning (Hospedales et al., 2020).

### 2.1. Supervised Learning

Many different works have striven to improve the performance of deep multi-task models. One line of research hypothesizes that conflicting per-task gradient directions lead to suboptimal models, and thus focuses on explicitly removing conflicts across task gradients (Yu et al., 2020; Chen et al., 2020; Liu et al., 2021; Wang et al., 2021). Some authors postulate that loss imbalances across tasks hinder learning, proposing loss reweighting methods (Kendall et al., 2018; Chen et al., 2018b; Lin et al., 2022). Finally, Sener & Koltun (2018) propose that tasks compete for model capacity and interpret MTL as multi-objective optimization in order to cope with inter-task competition (MGDA: see §4.2).

Here, we focus on algorithms that explicitly rely on per-task gradients to try to outperform unitary scalarization (§4). Research on multi-task architectures (Misra et al., 2016; Guo et al., 2020) or MTL algorithms exclusively motivated by deterministic loss reweighting (Kendall et al., 2018; Guo et al., 2018; Liu et al., 2019) are orthogonal to our work. Both topics are investigated by a recent survey on pixel-level multi-task computer vision problems (Vandenhende et al., 2021), which found the minimization of tuned weighted sums of losses to be empirically competitive with deterministic loss reweighting and MGDA in the considered settings.

### 2.2. Reinforcement Learning

We group multi-task RL research into three categories: the first adds auxiliary tasks providing additional inductive biases to speed up learning (Jaderberg et al., 2017) on a target task. The second, based on policy distillation, uses per-task teacher models to provide labels for a multi-task model or per-task policies as regularizers (Rusu et al., 2016; Parisotto et al., 2016; Teh et al., 2017a). The third directly learns a shared policy (Kalashnikov et al., 2021), possibly via a SMTO (Yu et al., 2020). We focus on the third category, whose literature reports varying performance for unitary scalarization (better (Kalashnikov et al., 2021) or worse (Yu et al., 2020) than per-task models), indicating confounding factors in evaluation pipelines and further motivating our work. PopArt (van Hasselt et al., 2016; Hessel et al., 2019) performs scale-invariant value function updates in order to address differences in returns across environments, showing improvements in the multi-task setting while still using unitary scalarization. PopArt does not require per-task gradients but introduces additional hyperparameters. In our work, we address the differences in rewards by normalizing them at the replay buffer level. However, we believe both unitary scalarization and other SMTOS might equally benefit from PopArt.

## 3. Multi-Task Learning

We denote the convex hull of a set  $\mathcal{A}$  by  $\text{Conv}(\mathcal{A})$ , and its affine hull by  $\text{Aff}(\mathcal{A})$ . Furthermore,  $\cos(\mathbf{x}, \mathbf{z})$  denotes the cosine similarity between vectors  $\mathbf{x}$  and  $\mathbf{z}$ ,  $[\mathbf{x}]_+ := \max(\mathbf{x}, \mathbf{0})$ ,  $\mathbf{1}_\mathbf{a}$  is the indicator vector on condition  $\mathbf{a}$ ,  $\text{sign}(\mathbf{x})$  stands for the element-wise sign operator applied on  $\mathbf{x}$ , and  $\odot$  denotes the Hadamard product.

Let  $(X, Y) \in \mathbb{R}^{d \times n} \times \mathbb{R}^{o \times n}$  be the training set, composed of  $n$   $d$ -dimensional points and  $o$ -dimensional labels. In addition,  $\mathcal{L}_i : \mathbb{R}^{o \times n} \times \mathbb{R}^{o \times n} \rightarrow \mathbb{R}$  denotes the loss for the  $i$ -th task,  $\theta \in \mathbb{R}^S$  the parameter space,  $\mathcal{T} := \{1, \dots, m\}$  the set of  $m$  tasks. The goal of MTL is to learn a single (generally task-aware) parametrized model  $f : \mathbb{R}^S \times \mathbb{R}^{d \times n} \times \mathcal{T} \rightarrow \mathbb{R}^{o \times n}$  that performs well on all tasks  $\mathcal{T}$ . The parameter space is often split into a set of

shared parameters across tasks (generally the majority of the architecture), denoted  $\theta_{\parallel}$ , and (possibly empty) task-specific parameters, denoted  $\theta_{\perp}$ , so that  $\theta := [\theta_{\parallel}, \theta_{\perp}]^T$ . In this context, the model  $f$  often takes on an encoder-decoder architecture, where the encoder  $g$  learns a shared representation across tasks, and the decoders  $h_i$  are task-specific predictive heads:  $f(\theta, X, i) = h_i(g(\theta_{\parallel}, X), \theta_{\perp})$ . In this case, we denote by  $\mathbf{z} = g(\theta_{\parallel}, X) \in \mathbb{R}^{n \times r}$  the  $r$ -dimensional shared representation of  $X$ .

The training problem for MTL is typically formulated as the sum of the per-task losses (Sener & Koltun, 2018; Yu et al., 2020; Chen et al., 2020):

$$\min_{\theta} \left[ \mathcal{L}^{\text{MT}}(\theta) := \sum_{i \in \mathcal{T}} \mathcal{L}_i(f(\theta, X, i), Y) \right]. \quad (1)$$

Equation (1) corresponds to a linear scalarization with unitary weights under a multi-objective interpretation of MTL; hence our “unitary scalarization” shorthand for the direct application of gradient descent on equation (1) (§4.1). While our presentation focuses, for simplicity, on standard gradient descent rather than mini-batch stochastic gradient descent, the notation can be easily adapted by replacing the dataset size  $n$  by the mini-batch size  $b$ .

## 4. Overview of Multi-Task Optimizers

In this section, we first start (§4.1) by outlining the standard way to tackle problem (1), then provide an overview of popular SMTOS: multiple-gradient descent algorithm (MGDA) (Sener & Koltun, 2018), impartial multi-task learning (IMTL) (Liu et al., 2021), PCGrad (Yu et al., 2020), and GradDrop (Chen et al., 2020). For each of these methods, we present theoretical results complementary to the original presentations, suggesting an alternative interpretation of these SMTOS as techniques that may reduce overfitting: in other words, regularizers (Dietterich, 1995). We refer the reader to appendix A for all proofs, to appendix C.2 and Figure 1 for empirical support of the interpretation.

Unless otherwise stated, we assume that MTL methods apply only to  $\theta_{\parallel}$  and that standard gradient-based updates are employed for tasks-specific parameters  $\theta_{\perp}$ . We furthermore adopt the following shorthands:  $\mathcal{L}_i(\theta)$  for  $\mathcal{L}_i(f(\theta, X, i), Y)$ , and  $\nabla_{\theta} \mathcal{L}_i$  for  $\nabla_{\theta} \mathcal{L}_i(f(\theta, X, i), Y)$ .

### 4.1. Unitary Scalarization

The obvious way to minimize the multi-task training objective in equation (1) is to rely on a standard gradient-based algorithm. For vanilla gradient descent, this corresponds to taking a step in the opposite direction as the one given by the sum of per-task gradients:  $\nabla_{\theta} \mathcal{L}^{\text{MT}} = \sum_{i \in \mathcal{T}} \nabla_{\theta} \mathcal{L}_i$ .

Per-task gradients are not required, as it suffices to directly

compute the gradient of the sum  $\mathcal{L}^{\text{MT}}$ . Hence, when relying on deep learning frameworks based on reverse-mode differentiation, such as PyTorch (Paszke et al., 2019), the backward pass is performed once per iteration (rather than  $m$  times). Furthermore, the memory cost is a factor  $m$  less than most SMTOS, which require access to each  $\nabla_{\theta} \mathcal{L}_i$ . As a consequence, unitary scalarization is simple, fast, and memory efficient. Our experiments demonstrate that, when possibly coupled with single-task regularization such as  $\ell_2$  penalty or dropout layers (Srivastava et al., 2014), this simple optimizer is strongly competitive with SMTOS.

### 4.2. MGDA

Sener & Koltun (2018) point out that equation (1) can be cast as a multi-objective optimization problem with the following objective:  $\mathcal{L}^{\text{MT}}(\theta) := [\mathcal{L}_1(\theta), \dots, \mathcal{L}_m(\theta)]^T$ . A commonly employed solution concept in multi-objective optimization is Pareto optimality. A point  $\theta^*$  is called Pareto-optimal if, for any other point  $\theta^{\dagger}$  such that  $\exists i \in \mathcal{T} : \mathcal{L}_i(\theta^{\dagger}) < \mathcal{L}_i(\theta^*)$ , then  $\exists j \in \mathcal{T} : \mathcal{L}_j(\theta^{\dagger}) > \mathcal{L}_j(\theta^*)$ . Sener & Koltun (2018) rely on MGDA (Désidéri, 2012) to reach a Pareto-optimal point for shared parameters  $\theta_{\parallel}$ . MGDA takes steps in a direction that decreases the loss of all tasks at once (Fliege & Svaiter, 2000; Désidéri, 2012), which can be found by solving the following optimization problem:

$$\min_{\mathbf{g}, \epsilon} \left[ \epsilon + \frac{1}{2} \|\mathbf{g}\|_2^2 \right] \quad \text{s.t. } \nabla_{\theta_{\parallel}} \mathcal{L}_i^T \mathbf{g} \leq \epsilon \quad \forall i \in \mathcal{T}, \quad (2)$$

whose dual takes the following form (corresponding to the formulation from Désidéri (2012)):

$$\begin{aligned} \max_{\alpha \geq 0} \quad & -\frac{1}{2} \|\mathbf{g}\|_2^2 \\ \text{s.t.} \quad & \sum_i \alpha_i \nabla_{\theta_{\parallel}} \mathcal{L}_i = -\mathbf{g}, \quad \sum_{i \in \mathcal{T}} \alpha_i = 1. \end{aligned} \quad (3)$$

In other words, MGDA takes a step in a direction  $\mathbf{g}$  given by the negative convex combination of per-task gradients, whose coefficients are given by solving equation (3). In practice, per-task gradients are rescaled before applying MGDA. We rely on  $\nabla_{\theta_{\parallel}} \mathcal{L}_i \leftarrow \nabla_{\theta_{\parallel}} \mathcal{L}_i / \|\nabla_{\theta_{\parallel}} \mathcal{L}_i\|_{\mathcal{L}_i(\theta)}$  as per the original authors’ implementation (Sener & Koltun, 2018). This prevents MGDA from assigning a large weight to the gradients that are smallest in magnitude, as instead claimed by Liu et al. (2021) when motivating the IMTL algorithm. The convergence of MGDA to a Pareto-optimal point is still guaranteed after normalization (Désidéri, 2012).

**Proposition 1.** *The MGDA SMTO by Sener & Koltun (2018) converges to a superset of the convergence points of unitary scalarization. More specifically, it converges to any point  $\theta_{\parallel}^*$  such that:  $0 \in \text{Conv}(\{\nabla_{\theta_{\parallel}} \mathcal{L}_i \mid i \in \mathcal{T}\})$ .*

As a consequence of Proposition 1, MGDA for MTL does not necessarily reach a stationary point for  $\mathcal{L}^{\text{MT}}$  (that is,

a point for which  $\sum_{i \in \mathcal{T}} \nabla_{\theta_{\parallel}} \mathcal{L}_i = \mathbf{0}$ ) or for any of the losses  $\mathcal{L}_i$  ( $\nabla_{\theta_{\parallel}} \mathcal{L}_i = \mathbf{0}$ ). For example, any point  $\theta_{\parallel}$  for which two per-task gradients point in opposite directions is Pareto optimal. On account of the well-known (Dietterich, 1995) relationship between under-optimizing (e.g., early stopping (Caruana et al., 2000)) and overfitting, we can then conclude that MGDA acts as a regularizer for equation (1).

### 4.3. IMTL

IMTL (Liu et al., 2021) is presented as an SMTD that is not biased against any single task. It is composed of two complementary algorithmic blocks: IMTL-L, acting on task losses, and IMTL-G, acting on per-task gradients.

IMTL-G follows the intuition that a multi-task optimizer should proceed along a direction  $\mathbf{g} = -\sum_i \alpha_i \nabla_{\theta_{\parallel}} \mathcal{L}_i$  that equally represents per-task gradients. This is formulated analytically by requiring that the cosine similarity between  $\mathbf{g}$  and each  $\nabla_{\theta_{\parallel}} \mathcal{L}_i$  be the same. To prevent the resulting problem from being underdetermined, Liu et al. (2021) add the constraint  $\sum_{i \in \mathcal{T}} \alpha_i = 1$ , resulting in a problem that admits a closed-form solution for  $\mathbf{g}$ :

$$\begin{aligned} \mathbf{g}^T \frac{\nabla_{\theta_{\parallel}} \mathcal{L}_1}{\|\nabla_{\theta_{\parallel}} \mathcal{L}_1\|} &= \mathbf{g}^T \frac{\nabla_{\theta_{\parallel}} \mathcal{L}_i}{\|\nabla_{\theta_{\parallel}} \mathcal{L}_i\|} \quad \forall i \in \mathcal{T} \setminus \{1\}, \\ \mathbf{g} &= -\sum_i \alpha_i \nabla_{\theta_{\parallel}} \mathcal{L}_i, \quad \sum_{i \in \mathcal{T}} \alpha_i = 1. \end{aligned} \quad (4)$$

IMTL-L, instead, aims to reweight task losses so that they are all constant over time, and equal to 1. In order to limit oscillations of the scaling factors, the authors propose to learn them jointly with the network by minimizing a common objective via gradient descent. In particular, given  $s_i \in \mathbb{R} \forall i \in \mathcal{T}$ , Liu et al. (2021) derive the following form for the joint minimization problem:  $\min_{\mathbf{s}, \theta} [\sum_i (e^{s_i} \mathcal{L}_i(\theta) - s_i)]$ . As proved by Liu et al. (2021), IMTL-L only has a rescaling effect on the update direction of IMTL-G. Unlike IMTL-G and the other SMTDs presented in this section, IMTL-L rescaling is designed to affect the updates for task-specific parameters  $\theta_{\perp}$  as well.

In the following, we first present an alternative interpretation of the update step of IMTL (Proposition 2), then analyze its convergence points (Corollary 1).

**Proposition 2.** IMTL by Liu et al. (2021) updates  $\theta_{\parallel}$  by taking a step in the steepest descent direction whose cosine similarity with per-task gradients is the same across tasks.

**Corollary 1.** IMTL by Liu et al. (2021) converges to a superset of the Pareto-optimal points for  $\theta_{\parallel}$  (and hence of the convergence points of the unitary scalarization). More specifically, it converges to any point  $\theta_{\parallel}^*$  such that:

$$\mathbf{0} \in \text{Aff} \left( \left\{ \frac{\nabla_{\theta_{\parallel}} \mathcal{L}_i}{\|\nabla_{\theta_{\parallel}} \mathcal{L}_i\|} \mid i \in \mathcal{T} \right\} \right).$$

As seen for MGDA (§4.2), Corollary 1 implies that, even if the employed model  $f$  has the capacity to reach the minimal loss on  $\mathcal{L}^{\text{MT}}$ , IMTL may stop before reaching a stationary point. Recalling the relationship between under-optimizing and overfitting (Dietterich, 1995), we conclude that IMTL also behaves as a regularizer for equation (1).

### 4.4. PCGrad

Yu et al. (2020) postulate that multi-task convergence is severely slowed down if the following three conditions (named the *tragic triad*) hold at once: (i) conflicting gradient directions:  $\cos(\nabla_{\theta_{\parallel}} \mathcal{L}_i, \nabla_{\theta_{\parallel}} \mathcal{L}_j) < 0$  for some  $i, j \in \mathcal{T}$ ; (ii) differing gradient magnitudes:  $\|\nabla_{\theta_{\parallel}} \mathcal{L}_i\| \gg \|\nabla_{\theta_{\parallel}} \mathcal{L}_j\|$  for some  $i, j \in \mathcal{T}$ ; and (iii) the unitary scalarization  $\mathcal{L}^{\text{MT}}$  has high curvature along  $\nabla_{\theta_{\parallel}} \mathcal{L}^{\text{MT}}$ .

The PCGrad (Yu et al., 2020) SMTD is presented as a solution to the tragic triad, targeted at the first condition. Consistent with the previous sections, let us denote the update direction by  $\mathbf{g}$ . Given per-task gradients  $\nabla_{\theta_{\parallel}} \mathcal{L}_i$ , PCGrad iteratively projects each task gradient onto the normal plane of all the gradients with which it conflicts:

$$\begin{aligned} \mathbf{g}_i &\leftarrow \nabla_{\theta_{\parallel}} \mathcal{L}_i, \\ \mathbf{g}_i &\leftarrow \mathbf{g}_i + \left[ \frac{-\mathbf{g}_i^T \nabla_{\theta_{\parallel}} \mathcal{L}_j(\mathbf{x})}{\|\nabla_{\theta_{\parallel}} \mathcal{L}_j\|^2} \right]_+ \nabla_{\theta_{\parallel}} \mathcal{L}_j, \quad \forall j \in \mathcal{T} \setminus \{i\} \quad \forall i \in \mathcal{T} \\ \mathbf{g} &= -\sum_{i \in \mathcal{T}} \mathbf{g}_i, \end{aligned} \quad (5)$$

where the iterative updates of  $\mathbf{g}_i$  with respect to  $\nabla_{\theta_{\parallel}} \mathcal{L}_j$  are performed in random order. We now provide an alternative characterization of the PCGrad update rule.

**Proposition 3.** PCGrad is equivalent to a dynamic, and possibly stochastic, loss rescaling for  $\theta_{\parallel}$ . In particular, at each iteration, per-task gradients are rescaled as follows:

$$\nabla_{\theta_{\parallel}} \mathcal{L}_i \leftarrow \left( 1 + \sum_{j \in \mathcal{T} \setminus \{i\}} d_{ji} \right) \nabla_{\theta_{\parallel}} \mathcal{L}_i,$$

with  $d_{ji} \in \left[ 0, \frac{\|\nabla_{\theta_{\parallel}} \mathcal{L}_j\|}{\|\nabla_{\theta_{\parallel}} \mathcal{L}_i\|} \right]$ . Furthermore, if  $|\mathcal{T}| > 2$ ,  $d_{ji}$  is a random variable, and the above range contains its support.

The results from proposition 3 can be easily extended to GradVac (Wang et al., 2021), which generalizes PCGrad's projection onto the normal vector to arbitrary target cosine similarities between per-task gradients. In line with the main technical results by Yu et al. (2020), we now restrict our focus to two-task problems, which allow for a better understanding of PCGrad's behavior.

**Corollary 2.** *If  $|\mathcal{T}| = 2$ , PCGrad will stop at any point where  $\cos(\nabla_{\theta_{\parallel}} \mathcal{L}_1, \nabla_{\theta_{\parallel}} \mathcal{L}_2) = -1$ . Furthermore, if  $\mathcal{L}_1$  and  $\mathcal{L}_2$  are differentiable, and  $\nabla_{\theta_{\parallel}} \mathcal{L}^{MT}$  is  $L$ -Lipschitz with  $L > 0$ , PCGrad with step size  $t < \frac{1}{L}$  converges to a superset of the convergence points of the unitary scalarization.*

Corollary 2 implies that, when  $|\mathcal{T}| = 2$ , PCGrad may induce early stopping on the unitary scalarization. This result mirrors those for MGDA (§4.2) and IMTL (§4.3). In particular, we note that, if  $\cos(\nabla_{\theta_{\parallel}} \mathcal{L}_1, \nabla_{\theta_{\parallel}} \mathcal{L}_2) = -1$ , then  $\mathbf{0} \in \text{Conv}(\{\nabla_{\theta_{\parallel}} \mathcal{L}_1, \nabla_{\theta_{\parallel}} \mathcal{L}_2\})$  (see proposition 1). When  $|\mathcal{T}| > 2$ , PCGrad corresponds to a stochastic loss re-weighting as shown by proposition 3. As such, PCGrad bears many similarities with a recently introduced Random Loss Weighting (RLW) (Lin et al., 2022). RLW proposes to sample scalarization weights from standard probability distributions at each iteration, and proves that this leads the better generalization (Lin et al., 2022, theorem 2). Indeed, it is well-known that adding noise to stochastic gradient estimations leads the optimization towards flatter minima, and that such minima may reduce overfitting (Keskar et al., 2017; Kleinberg et al., 2018). We hence conclude that PCGrad acts as a regularizer for any  $|\mathcal{T}|$ .

#### 4.5. GradDrop

Chen et al. (2020) focus on conflicting signs across task gradient entries, arguing that such conflicts lead to gradient “tug-of-wars”. The GradDrop SMTD (Chen et al., 2020), presented as a solution to this problem, proposes to randomly mask per-task gradients  $\nabla_{\theta_{\parallel}} \mathcal{L}_i$  so as to minimize such conflicts. Specifically, GradDrop computes the “positive sign purity”  $p_j$  for the task gradient’s  $j$ -th entry:

$$p_j = \frac{1}{2} \left( 1 + \frac{\sum_{i \in \mathcal{T}} \nabla_{\theta_{\parallel}} \mathcal{L}_i[j]}{\sum_{i \in \mathcal{T}} |\nabla_{\theta_{\parallel}} \mathcal{L}_i[j]|} \right),$$

and then masks the  $j$ -th entry of each per-task gradient with probability increasing with  $p_j$ , if the entry is negative, or decreasing with  $p_j$ , if the entry is positive. Let  $\mathbf{p} := [p_1, \dots, p_S]$ , where  $S$  is the dimensionality of the parameter space (see §3). Given a vector  $\mathbf{u}_i$ , uniformly sampled in  $[0, 1]$  at each iteration, GradDrop takes a step in the direction given by:

$$\mathbf{g} = \sum_{i \in \mathcal{T}} \begin{pmatrix} -\nabla_{\theta_{\parallel}} \mathcal{L}_i \odot \mathbf{1}_{(\nabla_{\theta_{\parallel}} \mathcal{L}_i > 0)} \odot \mathbf{1}_{(\mathbf{u}_i > \mathbf{p})} \\ -\nabla_{\theta_{\parallel}} \mathcal{L}_i \odot \mathbf{1}_{(\nabla_{\theta_{\parallel}} \mathcal{L}_i < 0)} \odot \mathbf{1}_{(\mathbf{u}_i < \mathbf{p})} \end{pmatrix}. \quad (6)$$

While the motivation behind GradDrop is to avoid entry-wise gradient conflicts across tasks, the main property of the method is to drive the optimization towards “joint minima”: points that are stationary for all the individual tasks at once (Chen et al., 2020, proposition 1). In other words:  $\nabla_{\theta_{\parallel}} \mathcal{L}_i = \mathbf{0} \forall i \in \mathcal{T}$ . We believe this property is indeed

desirable. However, we now show that it holds beyond GradDrop, and independently of the gradient directions. In particular, proposition 4 shows that, under strong assumptions on the model capacity, the above property would trivially hold for unitary scalarization. Proposition 5 shows that it holds for a simple randomized version of unitary scalarization.

**Proposition 4.** *Let us assume, as often demonstrated in the single-task case (Ma et al., 2018; Allen-Zhu et al., 2019), that the multi-task network has the capacity to interpolate the data on all tasks at once:  $\min_{\theta} \mathcal{L}^{MT} = \sum_{i \in \mathcal{T}} \min_{\theta} \mathcal{L}_i$ , and that its training by gradient descent attains such global minimum. Then, if  $\inf_{\theta} \mathcal{L}_i > -\infty \forall i \in \mathcal{T}$ , unitary scalarization converges to a joint minimum.*

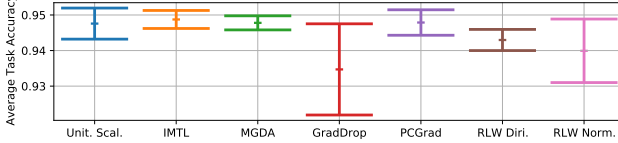
We refer to a sign-independent version of GradDrop as Random Grad Drop (RGD).

**Proposition 5.** *Let  $\mathcal{L}^{RGD}(\theta_{\parallel}) := \sum_{i \in \mathcal{T}} u_i \mathcal{L}_i(\theta_{\parallel})$ , where  $u_i \sim \text{Bernoulli}(p) \forall i \in \mathcal{T}$  and  $p \in (0, 1]$ . The gradient  $\nabla_{\theta_{\parallel}} \mathcal{L}^{RGD}$  is always zero if and only if  $\nabla_{\theta_{\parallel}} \mathcal{L}_i = \mathbf{0} \forall i \in \mathcal{T}$ . In other words, the result from (Chen et al., 2020, proposition 1) can be obtained without any information on the sign of per-task gradients.*

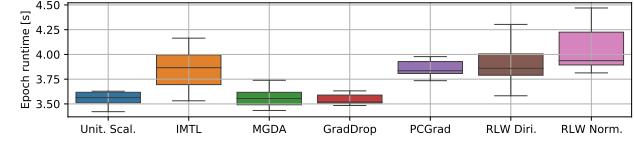
Proposition 5 shows that  $\mathcal{L}^{RGD}$ , an inexpensive stochastic scalarization, shares GradDrop’s main reported property. Similarly to PCGrad (§4.4), we can cast  $\mathcal{L}^{RGD}$  as an instance of RLW, and hence as a regularization method (Keskar et al., 2017; Kleinberg et al., 2018). Furthermore, appendix C.3 shows that the empirical results of GradDrop on CelebA (Liu et al., 2015) are closely matched by a sign-agnostic gradient masking, partly undermining the conflicting gradients assumption. We believe that the above results, along with the authors’ original experiments showing that GradDrop delays overfitting on CelebA (Chen et al., 2020, figure 3), suggest that GradDrop behaves as a regularizer.

## 5. Experiments

Our theoretical analysis (§4) provides a reinterpretation of SMTDs as implicit regularizers. As a consequence, the performance of unitary scalarization should match that of SMTDs when the former is adequately regularized. In order to test this hypothesis, we present an empirical evaluation on common MTL benchmarks of unitary scalarization (§4.1), the SMTDs presented in §4.2-§4.5, and the recent RLW algorithms (Lin et al., 2022) due to their similarities with PCGrad and GradDrop (see §4.4-4.5). In particular, we benchmark against the two RLW instances that showed the best average performance in the original paper: RLW with weights sampled from a Dirichlet distribution (“RLW Diri.”), and RLW with weights sampled from a Normal distribution (“RLW Norm.”). Whenever appropriate, we employ “Unit. Scal.” as shorthand for unitary scalarization. We first present supervised learning experiments (§5.1), and then evaluate



(a) Mean and 95% CI (10 runs) for the avg. task test accuracy.



(b) Box plots for the training time of a single epoch (10 repetitions).

Figure 2. In spite of larger overheads, no algorithm outperforms unitary scalarization on the Multi-MNIST dataset.

on a popular reinforcement learning benchmark (§5.2).

Our experiments indicate that the performance of unitary scalarization has been consistently underestimated in the literature. By showing the variability between runs and by relying on standard regularization and stabilization techniques from the single-task literature (see §4.1), we demonstrate that no SMT0 consistently outperforms unitary scalarization across the considered settings. This result holds in spite of the added complexity and computational overhead associated with most SMT0s. Furthermore, in supervised learning, most methods drive the training loss of all tasks in the proximity of the respective global minima. This suggests that the main difficulty of MTL is not associated to the optimization of its training problem, but rather to incorporating adequate regularization.

### 5.1. Supervised Learning

All the architectures employed in the supervised learning experiments conform to the encoder-decoder structure detailed in §3. Whenever suggested by the original authors for this context, the SMT0s implementations rely on per-task gradients with respect to the last shared activation,  $\nabla_z$ , rather than on the usually more expensive  $\nabla_\theta \mathcal{L}_i$ . In particular, this is the case for MGDA, IMTL and GradDrop. See appendix A for details concerning each individual algorithm. Surprisingly, several MTL works (Yu et al., 2020; Chen et al., 2020; Liu et al., 2021; Lin et al., 2022) report validation results instead of the test making it easier to overfit the validation dataset. Instead, following standard machine learning practice, we select a model on the validation set, and later report test metrics for all benchmarks. Validation results are also available in Appendix C. Appendix B.1 reports dataset descriptions, the computational setup, and hyperparameters omitted from this section.

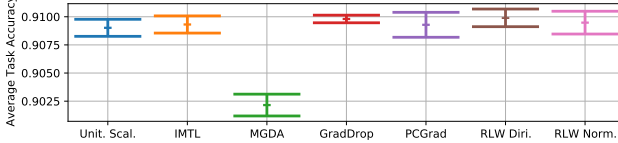
#### 5.1.1. MULTI-MNIST

We present results on the Multi-MNIST (Sener & Koltun, 2018) dataset, a simple two-task supervised learning benchmark. A single dropout layer (Srivastava et al., 2014) (with dropout probability 0.5) is employed in both the encoder and the decoder.  $\ell_2$  regularization did not improve validation performance and was therefore omitted. Figure 2a reports the average task test accuracy, and the training time per epoch. For each run, the test model was selected as the model with the largest average task validation accuracy across the training epochs. Appendix C presents the results of Figure 2 in tabular form, as well as the average task validation accuracy per epoch. As seen from the overlapping confidence intervals, none of the considered algorithms clearly outperforms the others. However, GradDrop displays higher experimental variability. Furthermore, Figure 7(c) shows that the sums of the task cross-entropy losses is driven nearly to zero by most methods. Finally, Figure 2(b) shows that unitary scalarization also has among the lowest training times.

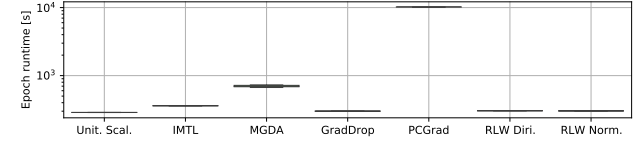
#### 5.1.2. CELEBA

We now show results for the CelebA (Liu et al., 2015) dataset, a challenging 40-task classification problem. Unlike previous multi-task experiments on this dataset, we tuned the addition of dropout layers, and considered non-zero  $\ell_2$  regularization terms  $\lambda$ . Specifically,  $\lambda = 10^{-3}$  yielded the best validation performance for unitary scalarization, IMTL and PCGrad, and  $\lambda = 10^{-4}$  for MGDA, GradDrop, and RLW. Validation performance was further stabilized by the addition of several dropout layers (see Figure 1), with dropout probabilities from 0.25 to 0.5. In order to assess the regularizing effect of SMT0s, Appendix C.2 and Figure 1 show additional results without regularization.

Analogously to our Multi-MNIST results, Figure 3 plots the



(a) Mean and 95% CI (3 runs) for the avg. task test accuracy.



(b) Box plots for the training time of a single epoch (10 repetitions).

Figure 3. While SMT0s display larger runtimes, none of them outperforms the unitary scalarization on the CelebA dataset.

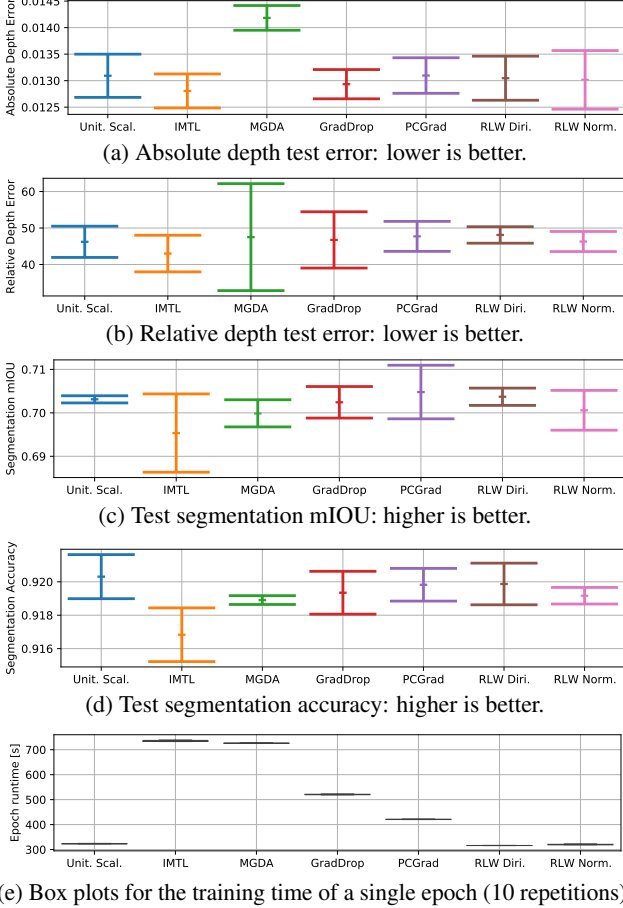


Figure 4. On Cityscapes, none of the SMTOS outperforms unitary scalarization, which proves to be the most cost-effective algorithm. Subfigures (a)-(d) report means for three runs, and their 95% CIs.

distribution of the training time per epoch, and the average test task accuracy. As with Multi-MNIST, the test model for each run was the one with maximal average validation task accuracy across epochs. Due to the large number of tasks, Figure 3(b) shows relatively large runtime differences across methods. PCGrad is the slowest (roughly 35 times slower than unitary scalarization). In fact, amongst the considered algorithms, it is the only one that computes per-task gradients over the parameters ( $\nabla_{\theta} \mathcal{L}_i \forall i \in \mathcal{T}$ ) at each iteration. GradDrop, MGDA and IMTL have overhead factors (compared to unitary scalarization) ranging from roughly 1.05 to 2.4 due to the relatively small size of  $\mathbf{z}$  for the employed architecture. The overhead of RLW is negligible: roughly 5%. Nevertheless, due to largely overlapping confidence intervals in Figure 3(a), none of the methods seems to consistently outperform unitary scalarization. In fact, its average performance is superior to the one reported in the literature (Sener & Koltun, 2018; Liu et al., 2021), testifying to insufficient regularization in this context. Furthermore, Figure 8(b) in Appendix C, plotting the average task accu-

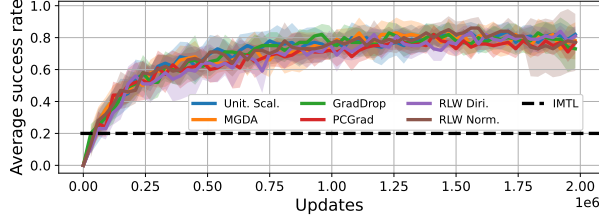
racy over the epochs, is consistent with the hypothesis that SMTOS implicitly act as regularizers: most of them either overfit less or require less regularization. We conjecture that the performance of unitary scalarization could be further improved by fine-tuning regularization parameters, such as the weight decay. Finally, as seen on Multi-MNIST, Figure 9(a) demonstrates that the cross-entropy loss of each task can be driven near to its global optimum by most optimizers.

### 5.1.3. CITYSCAPES

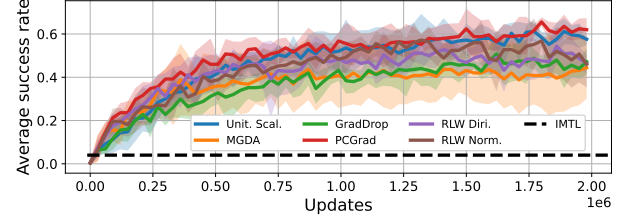
In order to complement the multi-task classification experiments for Multi-MNIST and CelebA, we present results for Cityscapes (Cordts et al., 2016), a dataset for semantic understanding of urban street scenes. A single dropout layer is contained in the task-specific heads. As for CelebA, we found unitary scalarization, IMTL, and PCGrad to benefit from more regularization than the other optimizers: we employ  $\lambda = 10^{-5}$  for these three algorithms, as it resulted in better validation performance on the majority of metrics, and  $\lambda = 0$  for the remaining methods. Figure 4 shows test results for two metrics per task, and the distribution of the training time per epoch. The test model for each run and each metric was selected as the one associated to the best (maximal or minimal, depending on the metric) validation result across epochs. As shown for the Multi-MNIST and CelebA datasets, no training algorithm clearly outperforms unitary scalarization (significant overlaps across confidence intervals exist), which is again shown to be the least expensive method. In contrast with a popular hypothesis (Kendall et al., 2018; Chen et al., 2018b; Liu et al., 2021), this holds in spite of relatively large loss imbalances. In fact, the loss for the depth task is roughly 10 times smaller than the one for the segmentation task: see figures 14(f)-14(f). Nevertheless, both losses are rapidly driven towards their respective global minima. Unlike CelebA (see Figure 3(b)), IMTL, MGDA and GradDrop are significantly slower than unitary scalarization (factors from 1.6 to 2.3), due to the relatively (compared to the parameter space) large size of  $\mathbf{z}$  in the employed architecture. PCGrad, instead, appears to be less expensive (30% more than the baseline), demonstrating the benefits of working on  $\nabla_{\theta} \mathcal{L}_i$  on this model.

## 5.2. Reinforcement Learning

For RL experiments, we use Meta-World (Yu et al., 2019) and the Soft Actor-Critic (Haarnoja et al., 2018) implementation from (Sodhani et al., 2021). Unlike §5.1, the employed network architecture (see appendix B.1) is fully shared across tasks. Therefore, all SMTOS implementations for these experiments rely on per-task gradients with respect to network parameters  $\nabla_{\theta} \mathcal{L}_i$  (see §4). Among the SMTOS we consider, PCGrad is the only one developed with the RL setting in mind. For fairness and completeness, we add all the other SMTOS from the supervised learning experiments,

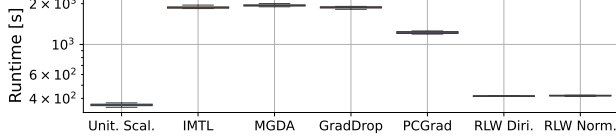


(a) MT10 (10 runs per method).

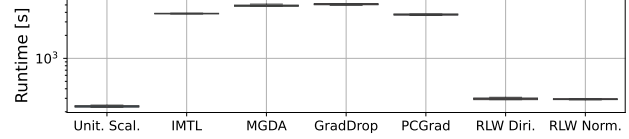


(b) MT50 (5 runs per method).

Figure 5. Mean and 95% CI for the avg. success rate on Metaworld. None of the SMTOS significantly outperforms unitary scalarization.



(a) MT10 (10 points per method).



(b) MT50 (10 points per method).

Figure 6. Box plots for the training time of 10,000 updates on Metaworld. Unitary scalarization is significantly faster than all SMTOS.

and are the first to test these optimizers in the RL setting.

To stabilize learning, we increase the replay buffer size, a well known technique in single-task RL, add actor  $l_2$  regularization, and modify the reward normalization employed by Sodhani et al. (2021). The unitary scalarization performance reported by Yu et al. (2020) is considerably lower than that of Sodhani et al. (2021), which we believe is due to the lack of reward normalization in the former. Sodhani et al. (2021) keep a moving average of rewards in the environment, with a hyperparameter controlling the speed of the moving average. As we show in Figure 13, the learning algorithm is sensitive to that hyperparameter. Moreover, such normalization might make similar transitions have drastically different rewards stored in the replay buffer. To alleviate these issues, we store the raw rewards in the buffer, and normalize only when a mini-batch is sampled. Our MT10 (10 tasks) results in Figure 5(a) show that by stabilizing the baseline using standard RL techniques, unitary scalarization performs on par with other SMTOS, mirroring our findings in §5.1. This is in contrast with the previous literature, which reported that PCGrad outperforms unitary scalarization (Yu et al., 2020; Sodhani et al., 2021). See Appendix B.2 for hyperparameter settings and ablation studies. We note that IMTL was found to be unstable on this RL benchmark: all of the runs crashed due to numerical overflow. In order to avoid incomplete curves and unfair calculations of the mean, we plot the highest value ever achieved by *any* seed as a dashed horizontal line. We hypothesize that the instability of IMTL is due to lack of bounds on scaling coefficients. Indeed, Liu et al. (2021) show that, in supervised settings, coefficients do not fluctuate much across epochs (Figure 4 in Appendix B in the original work) and never become negative. By contrast, up to 50% of the scaling coefficients  $\alpha$  are negative in our experiments, thus reverting subtask gradient directions.

Figure 5(b) presents results on MT50 (50 tasks): similarly to MT10, none of the SMTOS significantly outperforms unitary scalarization, with MGDA and GradDrop performing worse than on MT10. While we did not tune hyperparameters for MT50 (we employed those found for MT10), it would be much easier to do that for unitary scalarization due to its lower runtime. In fact, Figure 6(b) shows that a single unitary scalarization run takes roughly 15 hours, whereas PCGrad, MGDA and GradDrop require more than a week. Similarly to MT10, we noticed that actor regularization pushes unitary scalarization average performance higher (see in Appendix D.1). Overall, as in the supervised learning setting, unitary scalarization performs comparably to SMTOS despite being simpler and less demanding in both memory and compute.

## 6. Conclusion

This paper made two main contributions. First, we shed more light on existing SMTOS, providing an alternative interpretation of them as regularizers. Second, we evaluated them using a single experimental pipeline, including previously unpublished results of MGDA, IMTL, RLW, and GradDrop in the RL setting. Surprisingly, our evaluation showed that none of the SMTOS consistently outperform unitary scalarization, the simplest and least expensive method. This shows that the performance of unitary scalarization has been underestimated in the literature and calls for further reevaluation of progress in developing principled and efficient MTL algorithms.

## Acknowledgements

VK was funded by Samsung R&D Institute UK through the EPSRC Centre for Doctoral Training (CDT) in Autonomous Intelligent Machines and Systems (AIMS) at the University of Oxford. ADP was funded by EPSRC for the AIMS CDT, grant EP/L015987/1, and by an IBM PhD fellowship. SW has received funding from the European Research Council under the European Union’s Horizon 2020 research and innovation programme (grant agreement number 637713). The experiments were made possible by a generous equipment grant from NVIDIA. We would like to thank [Sodhani et al. \(2021\)](#); [Lin et al. \(2022\)](#) and [Sener & Koltun \(2018\)](#) for publicly releasing their code. The authors thank Kristian Hartikainen for helpful comments on the RL experiments.

## References

Allen-Zhu, Z., Li, Y., and Song, Z. A convergence theory for deep learning via over-parameterization. In *International Conference on Machine Learning*, 2019.

Bakker, B. and Heskes, T. Task clustering and gating for bayesian multitask learning. *Journal of Machine Learning Research*, 2003.

Cappart, Q., Chételat, D., Khalil, E. B., Lodi, A., Morris, C., and Velickovic, P. Combinatorial optimization and reasoning with graph neural networks. In *Proceedings of the Thirtieth International Joint Conference on Artificial Intelligence, IJCAI 2021, Virtual Event / Montreal, Canada, 19-27 August 2021*, 2021.

Caruana, R. Multitask learning. *Machine Learning*, 28(1): 41–75, 1997a.

Caruana, R. *Multitask learning*. PhD thesis, School of Computer Science, Carnegie Mellon University, Pittsburgh, PA 15213, 1997b.

Caruana, R., Lawrence, S., and Giles, L. Overfitting in neural nets: Backpropagation, conjugate gradient, and early stopping. In *Neural Information Processing Systems*, 2000.

Chen, L.-C., Zhu, Y., Papandreou, G., Schroff, F., and Adam, H. Encoder-decoder with atrous separable convolution for semantic image segmentation. In *European Conference on Computer Vision*, 2018a.

Chen, S., Zhang, Y., and Yang, Q. Multi-task learning in natural language processing: An overview. *CoRR*, 2021.

Chen, Z., Badrinarayanan, V., Lee, C.-Y., and Rabinovich, A. Gradnorm: Gradient normalization for adaptive loss balancing in deep multitask networks. In *International Conference on Machine Learning*, 2018b.

Chen, Z., Ngiam, J., Huang, Y., Luong, T., Kretzschmar, H., Chai, Y., and Anguelov, D. Just pick a sign: Optimizing deep multitask models with gradient sign dropout. In *Neural Information Processing Systems*, 2020.

Collobert, R. and Weston, J. A unified architecture for natural language processing: deep neural networks with multitask learning. In *Machine Learning, Proceedings of the Twenty-Fifth International Conference (ICML 2008), Helsinki, Finland, June 5-9, 2008*, 2008.

Cordts, M., Omran, M., Ramos, S., Rehfeld, T., Enzweiler, M., Benenson, R., Franke, U., Roth, S., and Schiele, B. The cityscapes dataset for semantic urban scene understanding. In *Conference on Computer Vision and Pattern Recognition*, 2016.

Désidéri, J. Multiple-gradient descent algorithm (MGDA) for multiobjective optimization. *Comptes Rendus Mathématique*, 350:313–318, 2012.

Dietterich, T. Overfitting and undercomputing in machine learning. *ACM Computing Surveys*, pp. 326–327, sep 1995.

Evgeniou, T. and Pontil, M. Regularized multi-task learning. In *ACM SIGKDD International Conference on Knowledge Discovery and Data Mining*, 2004.

Fliege, J. and Svaiter, B. F. Steepest descent methods for multicriteria optimization. *Mathematical Methods of Operations Research*, 2000.

Guo, M., Haque, A., Huang, D.-A., Yeung, S., and Fei-Fei, L. Dynamic task prioritization for multitask learning. In *Proceedings of the European Conference on Computer Vision (ECCV)*, September 2018.

Guo, P., Lee, C.-Y., and Ulbricht, D. Learning to branch for multi-task learning. 2020.

Haarnoja, T., Zhou, A., Abbeel, P., and Levine, S. Soft actor-critic: Off-policy maximum entropy deep reinforcement learning with a stochastic actor. In *International Conference on Machine Learning*, 2018.

He, K., Zhang, X., Ren, S., and Sun, J. Deep residual learning for image recognition. *Conference on Computer Vision and Pattern Recognition*, 2016.

Heskes, T. Empirical bayes for learning to learn. In *International Conference on Machine Learning*, 2000.

Hessel, M., Soyer, H., Espeholt, L., Czarnecki, W., Schmitt, S., and van Hasselt, H. Multi-task deep reinforcement learning with popart. In *The Thirty-Third AAAI Conference on Artificial Intelligence, AAAI 2019, The Thirty-First Innovative Applications of Artificial Intelligence*

*Conference, IAAI 2019, The Ninth AAAI Symposium on Educational Advances in Artificial Intelligence, EAAI 2019, Honolulu, Hawaii, USA, January 27 - February 1, 2019, pp. 3796–3803. AAAI Press, 2019.*

Hospedales, T. M., Antoniou, A., Micaelli, P., and Storkey, A. J. Meta-learning in neural networks: A survey. *CoRR*, 2020.

Huang, W., Mordatch, I., and Pathak, D. One policy to control them all: Shared modular policies for agent-agnostic control. In *Proceedings of the 37th International Conference on Machine Learning, ICML 2020, 13-18 July 2020, Virtual Event*, 2020.

Jaderberg, M., Mnih, V., Czarnecki, W. M., Schaul, T., Leibo, J. Z., Silver, D., and Kavukcuoglu, K. Reinforcement learning with unsupervised auxiliary tasks. In *5th International Conference on Learning Representations, ICLR 2017, Toulon, France, April 24-26, 2017, Conference Track Proceedings*. OpenReview.net, 2017.

Kalashnikov, D., Varley, J., Chebotar, Y., Swanson, B., Jonschkowski, R., Finn, C., Levine, S., and Hausman, K. Mt-opt: Continuous multi-task robotic reinforcement learning at scale. *CoRR*, 2021.

Kendall, A., Gal, Y., and Cipolla, R. Multi-task learning using uncertainty to weigh losses for scene geometry and semantics. In *Proceedings of the IEEE Conference on Computer Vision and Pattern Recognition (CVPR)*, 2018.

Keskar, N. S., Mudigere, D., Nocedal, J., Smelyanskiy, M., and Tang, P. T. P. On large-batch training for deep learning: Generalization gap and sharp minima. *International Conference on Learning Representations*, 2017.

Khetarpal, K., Riemer, M., Rish, I., and Precup, D. Towards continual reinforcement learning: A review and perspectives. *arXiv preprint arXiv:2012.13490*, 2020.

Kingma, D. P. and Ba, J. Adam: A method for stochastic optimization. In Bengio, Y. and LeCun, Y. (eds.), *International Conference on Learning Representations*, 2015.

Kleinberg, B., Li, Y., and Yuan, Y. An alternative view: When does SGD escape local minima? In *International Conference on Machine Learning*, 2018.

Kokkinos, I. Ubernet: Training a universal convolutional neural network for low-, mid-, and high-level vision using diverse datasets and limited memory. *IEEE Conference on Computer Vision and Pattern Recognition*, 2017.

Kurin, V., Godil, S., Whiteson, S., and Catanzaro, B. Can q-learning with graph networks learn a generalizable branching heuristic for a SAT solver? In *Advances in Neural Information Processing Systems 33: Annual Conference on Neural Information Processing Systems 2020, NeurIPS 2020, December 6-12, 2020, virtual*, 2020.

Kurin, V., Igl, M., Rocktäschel, T., Boehmer, W., and Whiteson, S. My body is a cage: the role of morphology in graph-based incompatible control. In *9th International Conference on Learning Representations, ICLR 2021, Virtual Event, Austria, May 3-7, 2021*, 2021.

LeCun, Y., Bottou, L., Bengio, Y., and Haffner, P. Gradient-based learning applied to document recognition. *IEEE*, 1998.

Lin, B., Ye, F., and Zhang, Y. A closer look at loss weighting in multi-task learning. 2022.

Liu, L., Li, Y., Kuang, Z., Xue, J.-H., Chen, Y., Yang, W., Liao, Q., and Zhang, W. Towards impartial multi-task learning. In *International Conference on Learning Representations*, 2021.

Liu, S., Johns, E., and Davison, A. J. End-to-end multi-task learning with attention. In *Proceedings of the IEEE Conference on Computer Vision and Pattern Recognition*, pp. 1871–1880, 2019.

Liu, Z., Luo, P., Wang, X., and Tang, X. Deep learning face attributes in the wild. In *Proceedings of International Conference on Computer Vision (ICCV)*, December 2015.

Ma, S., Bassily, R., and Belkin, M. The power of interpolation: Understanding the effectiveness of sgd in modern over-parametrized learning. In *International Conference on Machine Learning*, 2018.

Misra, I., Shrivastava, A., Gupta, A., and Hebert, M. Cross-stitch networks for multi-task learning. In *2016 IEEE Conference on Computer Vision and Pattern Recognition, CVPR 2016, Las Vegas, NV, USA, June 27-30, 2016*, 2016.

Narvekar, S., Peng, B., Leonetti, M., Sinapov, J., Taylor, M. E., and Stone, P. Curriculum learning for reinforcement learning domains: A framework and survey. *J. Mach. Learn. Res.*, 2020.

Parisotto, E., Ba, L. J., and Salakhutdinov, R. Actor-mimic: Deep multitask and transfer reinforcement learning. In Bengio, Y. and LeCun, Y. (eds.), *4th International Conference on Learning Representations, ICLR 2016, San Juan, Puerto Rico, May 2-4, 2016, Conference Track Proceedings*, 2016.

Paszke, A., Gross, S., Massa, F., Lerer, A., Bradbury, J., Chanan, G., Killeen, T., Lin, Z., Gimelshein, N., Antiga, L., Desmaison, A., Kopf, A., Yang, E., DeVito, Z., Raison, M., Tejani, A., Chilamkurthy, S., Steiner, B., Fang, L., Bai, J., and Chintala, S. Pytorch: An imperative

style, high-performance deep learning library. In *Neural Information Processing Systems*. 2019.

Rusu, A. A., Colmenarejo, S. G., Gülcühre, Ç., Desjardins, G., Kirkpatrick, J., Pascanu, R., Mnih, V., Kavukcuoglu, K., and Hadsell, R. Policy distillation. In Bengio, Y. and LeCun, Y. (eds.), *4th International Conference on Learning Representations, ICLR 2016, San Juan, Puerto Rico, May 2-4, 2016, Conference Track Proceedings*, 2016.

Seltzer, M. L. and Droppo, J. Multi-task learning in deep neural networks for improved phoneme recognition. In *IEEE International Conference on Acoustics, Speech and Signal Processing, ICASSP 2013, Vancouver, BC, Canada, May 26-31, 2013*, 2013.

Sener, O. and Koltun, V. Multi-task learning as multi-objective optimization. In *Neural Information Processing Systems*, 2018.

Sodhani, S., Zhang, A., and Pineau, J. Multi-task reinforcement learning with context-based representations. In Meila, M. and Zhang, T. (eds.), *International Conference on Machine Learning*, 2021.

Srivastava, N., Hinton, G., Krizhevsky, A., Sutskever, I., and Salakhutdinov, R. Dropout: A simple way to prevent neural networks from overfitting. *Journal of Machine Learning Research*, 2014.

Teh, Y. W., Bapst, V., Czarnecki, W. M., Quan, J., Kirkpatrick, J., Hadsell, R., Heess, N., and Pascanu, R. Distral: Robust multitask reinforcement learning. In Guyon, I., von Luxburg, U., Bengio, S., Wallach, H. M., Fergus, R., Vishwanathan, S. V. N., and Garnett, R. (eds.), *Advances in Neural Information Processing Systems 30: Annual Conference on Neural Information Processing Systems 2017, December 4-9, 2017, Long Beach, CA, USA*, pp. 4496–4506, 2017a.

Teh, Y. W., Bapst, V., Czarnecki, W. M., Quan, J., Kirkpatrick, J., Hadsell, R., Heess, N., and Pascanu, R. Distral: Robust multitask reinforcement learning. In *Neural Information Processing Systems*, 2017b.

van Hasselt, H. P., Guez, A., Hessel, M., Mnih, V., and Silver, D. Learning values across many orders of magnitude. *Advances in Neural Information Processing Systems*, 29: 4287–4295, 2016.

Vandenhende, S., Georgoulis, S., Van Gansbeke, W., Proesmans, M., Dai, D., and Van Gool, L. Multi-task learning for dense prediction tasks: A survey. *IEEE Transactions on Pattern Analysis and Machine Intelligence*, 2021.

Wang, Z., Tsvetkov, Y., Firat, O., and Cao, Y. Gradient vaccine: Investigating and improving multi-task optimization in massively multilingual models. In *International Conference on Learning Representations*, 2021.

Yu, F., Koltun, V., and Funkhouser, T. Dilated residual networks. In *Computer Vision and Pattern Recognition*, 2017.

Yu, T., Quillen, D., He, Z., Julian, R., Hausman, K., Finn, C., and Levine, S. Meta-world: A benchmark and evaluation for multi-task and meta reinforcement learning. In Kaelbling, L. P., Kragic, D., and Sugiura, K. (eds.), *3rd Annual Conference on Robot Learning*, 2019.

Yu, T., Kumar, S., Gupta, A., Levine, S., Hausman, K., and Finn, C. Gradient surgery for multi-task learning. 2020.

## A. Supplement to the Overview of Multi-Task Optimizers

This section presents the proofs and the technical results omitted from section 4, along with a description of the use of per-task gradients with respect to the last shared activation for encoder-decoder architectures (usually less expensive than per-task gradients with respect to shared parameters).

### A.1. MGDA

**Proposition 1.** *The MGDA SMTO by Sener & Koltun (2018) converges to a superset of the convergence points of unitary scalarization. More specifically, it converges to any point  $\theta_{\parallel}^*$  such that:  $\mathbf{0} \in \text{Conv}(\{\nabla_{\theta_{\parallel}} \mathcal{L}_i \mid i \in \mathcal{T}\})$ .*

*Proof.* Equation (3) is a simplex-constrained norm-minimization problem. In other words, the argument of the minimum is the projection of  $\mathbf{0}$  onto the feasible set. Therefore:

$$\mathbf{g} = \mathbf{0} \iff \mathbf{0} \in \text{Conv}(\{\nabla_{\theta_{\parallel}} \mathcal{L}_i \mid i \in \mathcal{T}\}).$$

It suffices to point out that  $\sum_{i \in \mathcal{T}} \nabla_{\theta_{\parallel}} \mathcal{L}_i = \mathbf{0} \iff \sum_{i \in \mathcal{T}} \frac{1}{|\mathcal{T}|} \nabla_{\theta_{\parallel}} \mathcal{L}_i = \mathbf{0} \Rightarrow \mathbf{0} \in \text{Conv}(\{\nabla_{\theta_{\parallel}} \mathcal{L}_i \mid i \in \mathcal{T}\})$  to conclude the proof.  $\square$

Due to the cost of computing per-task gradients, Sener & Koltun (2018) propose MGDA-UB, which replaces the gradients wrt the parameters  $\nabla_{\theta_{\parallel}} \mathcal{L}_i$  with the gradients wrt the shared activation  $\nabla_{\mathbf{z}} \mathcal{L}_i$  in the computation of the coefficients of  $\mathbf{g} = -\sum_i \alpha_i \nabla_{\theta_{\parallel}} \mathcal{L}_i$ . This yields an upper bound on the objective of equation (3), thus restricting the set of points the algorithm converges to. Rather than directly relying on  $\nabla_{\theta_{\parallel}} \mathcal{L}_i$ ,  $\mathbf{g}$  can then be obtained by computing the gradient of  $\sum_{i \in \mathcal{T}} \alpha_i \mathcal{L}_i$  via reverse-mode differentiation, hence saving memory and compute.

**Corollary 3.** *The MGDA-UB SMTO by Sener & Koltun (2018) converges to any point such that:  $\mathbf{0} \in \text{Conv}(\{\nabla_{\mathbf{z}} \mathcal{L}_i \mid i \in \mathcal{T}\})$ . Furthermore, if  $\frac{\partial \mathbf{z}}{\partial \theta_{\parallel}}$  is non-singular, it converges to a superset of the convergence points of the unitary scalarization.*

*Proof.* The first part of the proof proceeds as the proof of proposition 1, noting that the MGDA-UB update is associated to the following problem:

$$\begin{aligned} \max_{\alpha} \quad & -\frac{1}{2} \|\mathbf{g}\|_2^2 \\ \text{s.t.} \quad & \sum_i \alpha_i \nabla_{\mathbf{z}} \mathcal{L}_i = -\mathbf{g}, \quad \sum_{i \in \mathcal{T}} \alpha_i = 1, \\ & \alpha_i \geq 0 \quad \forall i \in \mathcal{T}. \end{aligned}$$

In order to show that a stationary point of the unitary scalarization satisfies  $\mathbf{0} \in \text{Conv}(\{\nabla_{\mathbf{z}^*} \mathcal{L}_i \mid i \in \mathcal{T}\})$ , we will

assume  $\frac{\partial \mathbf{z}}{\partial \theta_{\parallel}}$  is non-singular, as done by Sener & Koltun (2018, theorem 1). Then, relying on the chain rule, the result follows from:

$$\begin{aligned} \sum_{i \in \mathcal{T}} \nabla_{\theta_{\parallel}} \mathcal{L}_i = \mathbf{0} & \iff \sum_{i \in \mathcal{T}} \frac{1}{|\mathcal{T}|} \nabla_{\theta_{\parallel}} \mathcal{L}_i = \mathbf{0} \\ & \iff \sum_{i \in \mathcal{T}} \frac{\frac{\partial \mathbf{z}}{\partial \theta_{\parallel}}}{|\mathcal{T}|} \nabla_{\mathbf{z}} \mathcal{L}_i = \mathbf{0} \\ & \iff \left( \frac{\partial \mathbf{z}}{\partial \theta_{\parallel}} \right)^{-1} \frac{\partial \mathbf{z}}{\partial \theta_{\parallel}} \sum_{i \in \mathcal{T}} \frac{1}{|\mathcal{T}|} \nabla_{\mathbf{z}} \mathcal{L}_i = \mathbf{0} \\ & \iff \sum_{i \in \mathcal{T}} \frac{1}{|\mathcal{T}|} \nabla_{\mathbf{z}} \mathcal{L}_i = \mathbf{0} \\ & \Rightarrow \mathbf{0} \in \text{Conv}(\{\nabla_{\mathbf{z}} \mathcal{L}_i \mid i \in \mathcal{T}\}) \end{aligned}$$

$\square$

### A.2. IMTL

**Proposition 2.** *IMTL by Liu et al. (2021) updates  $\theta_{\parallel}$  by taking a step in the steepest descent direction whose cosine similarity with per-task gradients is the same across tasks.*

*Proof.* First, equation (4) solves the linear system in  $\alpha := [\alpha_1, \dots, \alpha_m]$  given by:

$$\begin{aligned} \mathbf{g}^T \left( \frac{\nabla_{\theta_{\parallel}} \mathcal{L}_1}{\|\nabla_{\theta_{\parallel}} \mathcal{L}_1\|} - \frac{\nabla_{\theta_{\parallel}} \mathcal{L}_i}{\|\nabla_{\theta_{\parallel}} \mathcal{L}_i\|} \right) &= \mathbf{0} \quad \forall i \in \mathcal{T} \setminus \{1\}, \\ \mathbf{g} = -\sum_i \alpha_i \nabla_{\theta_{\parallel}} \mathcal{L}_i, \quad \sum_{i \in \mathcal{T}} \alpha_i &= 1, \end{aligned}$$

which corresponds to finding a point of  $\mathcal{A}' := \text{Aff}(\{\nabla_{\theta_{\parallel}} \mathcal{L}_i \mid i \in \mathcal{T}\})$  which is orthogonal to  $\mathcal{A} := \text{Aff} \left( \left\{ \frac{\nabla_{\theta_{\parallel}} \mathcal{L}_i}{\|\nabla_{\theta_{\parallel}} \mathcal{L}_i\|} \mid i \in \mathcal{T} \right\} \right)$ . To see this, it suffices to point out that any point orthogonal to  $\mathcal{A}$  is also orthogonal to the vector subspace spanned by differences of vectors belonging to  $\mathcal{A}$ . As this subspace has  $m-1$  dimensions, any vector orthogonal to  $\left( \frac{\nabla_{\theta_{\parallel}} \mathcal{L}_1}{\|\nabla_{\theta_{\parallel}} \mathcal{L}_1\|} - \frac{\nabla_{\theta_{\parallel}} \mathcal{L}_i}{\|\nabla_{\theta_{\parallel}} \mathcal{L}_i\|} \right)$  for each  $i \in \mathcal{T} \setminus \{1\}$  is orthogonal to the entire subspace.

Second, consider the problem of finding a point in  $\mathcal{A}$  that is orthogonal to the affine subspace  $\mathcal{A}'$ . In other words, we seek the projection of  $\mathbf{0}$  onto  $\mathcal{A}$ . Recalling the definition of  $\mathcal{A}$ , we can write:

$$\begin{aligned} \max_{\alpha} \quad & -\frac{1}{2} \|\mathbf{g}'\|_2^2 \\ \text{s.t.} \quad & \sum_i \alpha_i \frac{\nabla_{\theta_{\parallel}} \mathcal{L}_i}{\|\nabla_{\theta_{\parallel}} \mathcal{L}_i\|} = -\mathbf{g}', \quad \sum_i \alpha_i = 1. \end{aligned} \tag{7}$$

The solution of equation (7) is always collinear to the solution of equation (4). In fact, if a vector  $\mathbf{g} \in \mathcal{A}'$

is orthogonal to the affine subspace  $\mathcal{A}$ , then  $\gamma \mathbf{g} = \left( \gamma \sum_i (\alpha_i \|\nabla_{\theta_{\parallel}} \mathcal{L}_i\|) \frac{\nabla_{\theta_{\parallel}} \mathcal{L}_i}{\|\nabla_{\theta_{\parallel}} \mathcal{L}_i\|} \right)$  is orthogonal to  $\mathcal{A}$  as well, and  $\gamma = \frac{1}{\sum_i (\alpha_i \|\nabla_{\theta_{\parallel}} \mathcal{L}_i\|)} \implies \gamma \mathbf{g} \in \mathcal{A}$ .

Finally, equation (7) differs from equation (3) in two aspects:  $\alpha$  is not constrained to be non-negative (hence the convex hull is replaced by the affine hull), and the task vectors are normalized. Therefore, equation (7) is the dual of:

$$\begin{aligned} \min_{\mathbf{g}, \epsilon} \quad & \epsilon + \frac{1}{2} \|\mathbf{g}\|_2^2 \\ \text{s.t.} \quad & \frac{\nabla_{\theta_{\parallel}} \mathcal{L}_i^T}{\|\nabla_{\theta_{\parallel}} \mathcal{L}_i\|} \mathbf{g} = \epsilon \quad \forall i \in \llbracket 1, m \rrbracket. \end{aligned} \quad (8)$$

The proposition then follows by comparing equation (8) with equation (2), and recalling that IMTL-L only adds a scaling factor to the chosen update direction.  $\square$

**Corollary 1.** IMTL by Liu et al. (2021) converges to a superset of the Pareto-optimal points for  $\theta_{\parallel}$  (and hence of the convergence points of the unitary scalarization). More specifically, it converges to any point  $\theta_{\parallel}^*$  such that:

$$\mathbf{0} \in \text{Aff} \left( \left\{ \frac{\nabla_{\theta_{\parallel}} \mathcal{L}_i}{\|\nabla_{\theta_{\parallel}} \mathcal{L}_i\|} \mid i \in \mathcal{T} \right\} \right).$$

*Proof.* Inspecting equation (8), which yields a collinear point to the IMTL update, reveals that IMTL might converge to non Pareto-stationary points: due to the restrictive equality constraints, the minimizer of equation (8) might be  $\mathbf{0}$  even if a descent direction exists. Furthermore, its dual, equation (7), implies that:

$$\begin{aligned} \mathbf{g} = \mathbf{0} \iff & \mathbf{0} \in \text{Aff} \left( \left\{ \frac{\nabla_{\theta_{\parallel}} \mathcal{L}_i}{\|\nabla_{\theta_{\parallel}} \mathcal{L}_i\|} \mid i \in \mathcal{T} \right\} \right) \\ \iff & \mathbf{0} \in \text{Aff} \left( \left\{ \nabla_{\theta_{\parallel}} \mathcal{L}_i \mid i \in \mathcal{T} \right\} \right), \end{aligned}$$

which, noting that  $\text{Conv}(\mathcal{A}) \subseteq \text{Aff}(\mathcal{A})$  for any  $\mathcal{A}$ , concludes the proof.  $\square$

Similarly to MGDA-UB, Liu et al. (2021) advocate using  $\nabla_{\mathbf{z}} \mathcal{L}_i$  in place of  $\nabla_{\theta_{\parallel}} \mathcal{L}_i$  while solving equation (4), typically reducing the cost of computing the coefficients of  $\mathbf{g} = -\sum_i \alpha_i \nabla_{\theta_{\parallel}} \mathcal{L}_i$ .

**Corollary 4.** When employing the approximation of problem (4) that relies on  $\nabla_{\mathbf{z}} \mathcal{L}_i$ , IMTL by Liu et al. (2021) converges to  $\mathbf{0} \in \text{Aff} \left( \left\{ \frac{\nabla_{\mathbf{z}} \mathcal{L}_i}{\|\nabla_{\mathbf{z}} \mathcal{L}_i\|} \mid i \in \mathcal{T} \right\} \right)$ . If  $\frac{\partial \mathbf{z}}{\partial \theta_{\parallel}}$  is non-singular, this is a superset of the convergence points of the unitary scalarization.

*Proof.* Following the proof of proposition 2, the following problem yields a collinear point to the  $\nabla_{\mathbf{z}} \mathcal{L}_i$ -approximate IMTL update:

$$\begin{aligned} \max_{\alpha} \quad & -\frac{1}{2} \|\mathbf{g}'\|_2^2 \\ \text{s.t.} \quad & \sum_i \alpha_i \frac{\nabla_{\mathbf{z}} \mathcal{L}_i}{\|\nabla_{\mathbf{z}} \mathcal{L}_i\|} = -\mathbf{g}', \quad \sum_i \alpha_i = 1. \end{aligned}$$

Therefore:

$$\mathbf{g} = \mathbf{0} \iff \mathbf{0} \in \text{Aff} \left( \left\{ \frac{\nabla_{\mathbf{z}} \mathcal{L}_i}{\|\nabla_{\mathbf{z}} \mathcal{L}_i\|} \mid i \in \mathcal{T} \right\} \right).$$

Finally, assuming  $\frac{\partial \mathbf{z}}{\partial \theta_{\parallel}}$  is non-singular, we can replicate the procedure in the proof of corollary 3 to get:

$$\begin{aligned} \sum_{i \in \mathcal{T}} \nabla_{\theta_{\parallel}} \mathcal{L}_i = \mathbf{0} \iff & \sum_{i \in \mathcal{T}} \frac{1}{|\mathcal{T}|} \nabla_{\mathbf{z}} \mathcal{L}_i = \mathbf{0} \\ \iff & \sum_{i \in \mathcal{T}} \frac{\|\nabla_{\mathbf{z}} \mathcal{L}_i\|}{|\mathcal{T}|} \frac{\nabla_{\mathbf{z}} \mathcal{L}_i}{\|\nabla_{\mathbf{z}} \mathcal{L}_i\|} = \mathbf{0} \\ \iff & \left( \frac{|\mathcal{T}|}{\sum_{i \in \mathcal{T}} (\|\nabla_{\mathbf{z}} \mathcal{L}_i\|)} \right) \sum_{i \in \mathcal{T}} \frac{\|\nabla_{\mathbf{z}} \mathcal{L}_i\|}{|\mathcal{T}|} \frac{\nabla_{\mathbf{z}} \mathcal{L}_i}{\|\nabla_{\mathbf{z}} \mathcal{L}_i\|} = \mathbf{0} \\ \Rightarrow & \mathbf{0} \in \text{Conv} \left( \left\{ \frac{\nabla_{\mathbf{z}} \mathcal{L}_i}{\|\nabla_{\mathbf{z}} \mathcal{L}_i\|} \mid i \in \mathcal{T} \right\} \right) \\ \Rightarrow & \mathbf{0} \in \text{Aff} \left( \left\{ \frac{\nabla_{\mathbf{z}} \mathcal{L}_i}{\|\nabla_{\mathbf{z}} \mathcal{L}_i\|} \mid i \in \mathcal{T} \right\} \right), \end{aligned}$$

which shows that  $\text{Aff} \left( \left\{ \frac{\nabla_{\mathbf{z}} \mathcal{L}_i}{\|\nabla_{\mathbf{z}} \mathcal{L}_i\|} \mid i \in \mathcal{T} \right\} \right)$  contains the convergence points of the unitary scalarization.  $\square$

### A.3. PCGrad

**Proposition 3.** PCGrad is equivalent to a dynamic, and possibly stochastic, loss rescaling for  $\theta_{\parallel}$ . In particular, at each iteration, per-task gradients are rescaled as follows:

$$\nabla_{\theta_{\parallel}} \mathcal{L}_i \leftarrow \left( 1 + \sum_{j \in \mathcal{T} \setminus \{i\}} d_{ji} \right) \nabla_{\theta_{\parallel}} \mathcal{L}_i,$$

with  $d_{ji} \in \left[ 0, \frac{\|\nabla_{\theta_{\parallel}} \mathcal{L}_j\|}{\|\nabla_{\theta_{\parallel}} \mathcal{L}_i\|} \right]$ . Furthermore, if  $|\mathcal{T}| > 2$ ,  $d_{ji}$  is a random variable, and the above range contains its support.

*Proof.* We start by pointing out that:

$$\begin{aligned} \left[ \frac{-\mathbf{g}_i^T \nabla_{\theta_{\parallel}} \mathcal{L}_j(\mathbf{x})}{\|\nabla_{\theta_{\parallel}} \mathcal{L}_j\|^2} \right]_+ &= \left[ \frac{-\mathbf{g}_i^T \nabla_{\theta_{\parallel}} \mathcal{L}_j(\mathbf{x})}{\|\nabla_{\theta_{\parallel}} \mathcal{L}_j\|} \right]_+ \frac{1}{\|\nabla_{\theta_{\parallel}} \mathcal{L}_j\|} \\ &= [-\cos(\mathbf{g}_i, \nabla_{\theta_{\parallel}} \mathcal{L}_j) \|\mathbf{g}_i\|]_+ \frac{1}{\|\nabla_{\theta_{\parallel}} \mathcal{L}_j\|} \\ &\in \left[ 0, \frac{\|\mathbf{g}_i\|}{\|\nabla_{\theta_{\parallel}} \mathcal{L}_j\|} \right]. \end{aligned}$$

As  $\mathbf{g}_i$  is obtained by iterative projections of  $\nabla_{\theta_{\parallel}} \mathcal{L}_i$  onto the normals of  $\nabla_{\theta_{\parallel}} \mathcal{L}_j \forall j \in \mathcal{T} \setminus \{i\}$ , and the norm of a vector can only decrease or remain unvaried after projections, we can write the coefficient of the last  $\mathbf{g}_i$  update as:

$$d_{ij} := \left[ \frac{-\mathbf{g}_i^T \nabla_{\theta_{\parallel}} \mathcal{L}_j(\mathbf{x})}{\|\nabla_{\theta_{\parallel}} \mathcal{L}_j\|^2} \right]_+ \in \left[ 0, \frac{\|\nabla_{\theta_{\parallel}} \mathcal{L}_i\|}{\|\nabla_{\theta_{\parallel}} \mathcal{L}_j\|} \right].$$

Furthermore, if  $|\mathcal{T}| > 2$  the contraction factor  $\frac{\|\mathbf{g}_i\|}{\|\nabla_{\theta_{\parallel}} \mathcal{L}_i\|}$  for the norm of  $\mathbf{g}_i$  depends on the ordering of the projections, which is stochastic by design (Yu et al., 2020). Therefore,  $d_{ij}$  a random variable whose support is contained in  $\left[ 0, \frac{\|\nabla_{\theta_{\parallel}} \mathcal{L}_i\|}{\|\nabla_{\theta_{\parallel}} \mathcal{L}_j\|} \right]$ . Finally, exploiting the definition of  $d_{ij}$ , we can re-write equation (5) as:

$$\begin{aligned} -\mathbf{g} &= \sum_{i \in \mathcal{T}} \nabla_{\theta_{\parallel}} \mathcal{L}_i + \sum_{i \in \mathcal{T}} \sum_{j \in \mathcal{T} \setminus \{i\}} d_{ij} \\ &= \sum_{i \in \mathcal{T}} \nabla_{\theta_{\parallel}} \mathcal{L}_i + \sum_{j \in \mathcal{T}} \sum_{i \in \mathcal{T} \setminus \{j\}} d_{ji} \\ &= \sum_{i \in \mathcal{T}} \nabla_{\theta_{\parallel}} \mathcal{L}_i \left( 1 + \sum_{j \in \mathcal{T} \setminus \{i\}} d_{ji} \right), \end{aligned}$$

from which the result trivially follows.  $\square$

**Corollary 2.** *If  $|\mathcal{T}| = 2$ , PCGrad will stop at any point where  $\cos(\nabla_{\theta_{\parallel}} \mathcal{L}_1, \nabla_{\theta_{\parallel}} \mathcal{L}_2) = -1$ . Furthermore, if  $\mathcal{L}_1$  and  $\mathcal{L}_2$  are differentiable, and  $\nabla_{\theta_{\parallel}} \mathcal{L}^{\text{MT}}$  is  $L$ -Lipschitz with  $L > 0$ , PCGrad with step size  $t < \frac{1}{L}$  converges to a superset of the convergence points of the unitary scalarization.*

*Proof.* Let us start from the first statement, which does not require any assumption on the loss landscape. From proposition 3, we get:

$$\begin{aligned} -\mathbf{g} &= \nabla_{\theta_{\parallel}} \mathcal{L}_1 (1 + d_{21}) + \nabla_{\theta_{\parallel}} \mathcal{L}_2 (1 + d_{12}) \\ &= \left( 1 + \left[ \frac{-\cos(\nabla_{\theta_{\parallel}} \mathcal{L}_1, \nabla_{\theta_{\parallel}} \mathcal{L}_2) \|\nabla_{\theta_{\parallel}} \mathcal{L}_2\|}{\|\nabla_{\theta_{\parallel}} \mathcal{L}_1\|} \right]_+ \right) \nabla_{\theta_{\parallel}} \mathcal{L}_1 \\ &\quad + \left( 1 + \left[ \frac{-\cos(\nabla_{\theta_{\parallel}} \mathcal{L}_1, \nabla_{\theta_{\parallel}} \mathcal{L}_2) \|\nabla_{\theta_{\parallel}} \mathcal{L}_1\|}{\|\nabla_{\theta_{\parallel}} \mathcal{L}_2\|} \right]_+ \right) \nabla_{\theta_{\parallel}} \mathcal{L}_2, \end{aligned}$$

which shows that, in case of conflicting gradient directions, gradient norms are rebalanced proportionally to the angle between them. For  $\cos(\nabla_{\theta_{\parallel}} \mathcal{L}_1, \nabla_{\theta_{\parallel}} \mathcal{L}_2) = -1$ , the above evaluates to:

$$\begin{aligned} -\mathbf{g} &= \left( \frac{\|\nabla_{\theta_{\parallel}} \mathcal{L}_1\| + \|\nabla_{\theta_{\parallel}} \mathcal{L}_2\|}{\|\nabla_{\theta_{\parallel}} \mathcal{L}_1\|} \right) \nabla_{\theta_{\parallel}} \mathcal{L}_1 \\ &\quad + \left( \frac{\|\nabla_{\theta_{\parallel}} \mathcal{L}_1\| + \|\nabla_{\theta_{\parallel}} \mathcal{L}_2\|}{\|\nabla_{\theta_{\parallel}} \mathcal{L}_2\|} \right) \nabla_{\theta_{\parallel}} \mathcal{L}_2. \end{aligned}$$

The first part of the result then follows by pointing out that, if  $\cos(\nabla_{\theta_{\parallel}} \mathcal{L}_1, \nabla_{\theta_{\parallel}} \mathcal{L}_2) = -1$ , then  $\nabla_{\theta_{\parallel}} \mathcal{L}_1 = -\nabla_{\theta_{\parallel}} \mathcal{L}_2$ , and hence  $\mathbf{g} = \mathbf{0}$ . We remark that a similar proof appears in (Yu et al., 2020, theorem 1 and proposition 1). However, our derivation relaxes the author's assumptions on  $\mathcal{L}^{\text{MT}}$  and is therefore applicable to the training of neural networks.

Finally, given the assumptions on differentiability and smoothness, we need to prove that PCGrad converges to the stationary points of the unitary scalarization: this directly follows from (Yu et al., 2020, proposition 1).  $\square$

#### A.4. GradDrop

**Proposition 4.** *Let us assume, as often demonstrated in the single-task case (Ma et al., 2018; Allen-Zhu et al., 2019), that the multi-task network has the capacity to interpolate the data on all tasks at once:  $\min_{\theta} \mathcal{L}^{\text{MT}} = \sum_{i \in \mathcal{T}} \min_{\theta} \mathcal{L}_i$ , and that its training by gradient descent attains such global minimum. Then, if  $\inf_{\theta} \mathcal{L}_i > -\infty \forall i \in \mathcal{T}$ , unitary scalarization converges to a joint minimum.*

*Proof.* It suffices to point out that if  $\mathcal{L}^{\text{MT}}(\theta^*) = \sum_{i \in \mathcal{T}} \min_{\theta} \mathcal{L}_i$ , then the globally optimal loss is attained for all tasks. In other words  $\mathcal{L}_i(\theta^*) = \min_{\theta} \mathcal{L}_i \forall i \in \mathcal{T}$ , and hence  $\nabla_{\theta^*} \mathcal{L}_i = \mathbf{0} \forall i \in \mathcal{T}$  (joint minimum). Furthermore, running gradient descent on  $\min_{\theta} \mathcal{L}^{\text{MT}}$  corresponds to the unitary scalarization (§4.1), which concludes the proof.  $\square$

**Proposition 5.** *Let  $\mathcal{L}^{\text{RGD}}(\theta_{\parallel}) := \sum_{i \in \mathcal{T}} u_i \mathcal{L}_i(\theta_{\parallel})$ , where  $u_i \sim \text{Bernoulli}(p) \forall i \in \mathcal{T}$  and  $p \in (0, 1]$ . The gradient  $\nabla_{\theta_{\parallel}} \mathcal{L}^{\text{RGD}}$  is always zero if and only if  $\nabla_{\theta_{\parallel}} \mathcal{L}_i = \mathbf{0} \forall i \in \mathcal{T}$ . In other words, the result from (Chen et al., 2020, proposition 1) can be obtained without any information on the sign of per-task gradients.*

*Proof.* Let us start from the statement on  $\nabla_{\theta_{\parallel}} \mathcal{L}^{\text{RGD}}$ . If  $\nabla_{\theta_{\parallel}} \mathcal{L}_i = \mathbf{0} \forall i \in \mathcal{T}$ , then  $\nabla_{\theta_{\parallel}} \mathcal{L}^{\text{RGD}} = \mathbf{0}$  with probability one. On the other hand, if  $\exists j : \nabla_{\theta_{\parallel}} \mathcal{L}_j \neq \mathbf{0}$ , then:

$$\begin{aligned} \mathbb{P} [\nabla_{\theta_{\parallel}} \mathcal{L}^{\text{RGD}} \neq \mathbf{0}] &\geq \mathbb{P} [\nabla_{\theta_{\parallel}} \mathcal{L}^{\text{RGD}} = \nabla_{\theta_{\parallel}} \mathcal{L}_j] \\ &= p(1-p)^{m-1} > 0, \end{aligned}$$

where the first inequality comes from the fact that  $\nabla_{\theta_{\parallel}} \mathcal{L}^{\text{RGD}} = \nabla_{\theta_{\parallel}} \mathcal{L}_j$  is only one of the many instances of a non-null  $\nabla_{\theta_{\parallel}} \mathcal{L}^{\text{RGD}}$ .  $\square$

On encoder-decoder architectures, similarly to MGDA (§4.2) and IMTL (§4.3), the authors do not apply GradDrop on  $\nabla_{\theta_{\parallel}} \mathcal{L}_i$ , but rather on the a the usually less expensive  $\nabla_{\mathbf{z}} \mathcal{L}_i$ . In more detail, they compute the GradDrop sign purity scores  $\mathbf{p}$  from equation (6) on  $\sum_{i=1}^n (\text{sign}(\mathbf{z}) \odot \nabla_{\mathbf{z}} \mathcal{L}_i)[i] \in \mathbb{R}^r$ , and then apply equation (6) on the  $\nabla_{\mathbf{z}} \mathcal{L}_i$  gradients, yielding a vector  $\mathbf{g}_z \in \mathbb{R}^{n \times r}$ . Then, relying on reverse-mode differentiation, the update direction in the space of

the parameters  $\theta_{\parallel}$  is obtained via a Jacobian-vector product:  $\mathbf{g} = -\left(\frac{\partial \mathbf{z}}{\partial \theta_{\parallel}}\right)^T \mathbf{g}_z$ . Such a computation replaces the similar  $\nabla_{\theta_{\parallel}} \mathcal{L}^{\text{MT}} = \left(\frac{\partial \mathbf{z}}{\partial \theta_{\parallel}}\right)^T \nabla_{\mathbf{z}} \mathcal{L}^{\text{MT}}$  from the unitary scalarization.

## B. Experimental Setting, Reproducibility

We now present details concerning the experimental settings from §5, including dataset details, hardware specifications, and hyper-parameters.

### B.1. Supervised Learning

All the experiments were run under Ubuntu 18.04 LTS, on a single GPU per run. Timing experiments were all run on Nvidia GeForce GTX 1080 Ti GPUs, with an Intel Xeon E5-2650 CPU. The remaining experiments were run on either Nvidia GeForce RTX 2080 Ti GPUs or Nvidia GeForce GTX 1080 Ti GPUs, respectively using an Intel Xeon Gold 6230 CPU or an Intel Xeon E5-2650 CPU.

#### B.1.1. MULTIMNIST

Multi-MNIST (Sener & Koltun, 2018) is a simple two-task supervised learning benchmark dataset constructed by uniformly sampling MNIST (LeCun et al., 1998) images, and placing one in the top-left corner, the other in the bottom-right corner. Each of the two overlaid images corresponds to a 10-class classification task. Using the above procedure, we generate the Multi-MNIST training set from the first 50000 MNIST training images, the validation set from the last 10000 training images, and the test set from the original MNIST test set. For consistency with the experimental setup of Sener & Koltun (2018), we employ a modified encoder-decoder version of the LeNet architecture (LeCun et al., 1998). Specifically, the last layer is omitted from the encoder, and two fully-connected layers are employed as task-specific predictive heads. The cross-entropy loss is used for both tasks. All methods are trained for 100 epochs using Adam (Kingma & Ba, 2015) in the stochastic gradient setting, with an initial learning rate of  $\eta = 10^{-2}$  (yielding the best validation results for all considered algorithms), exponentially decayed by 0.95 after each epoch, and a mini-batch size of 256.

#### B.1.2. CELEBA

The CelebA (Liu et al., 2015) dataset consists of 200,000 headshots (with standard training, validation and test splits) associated with the presence or absence of 40 attributes. In the MTL literature, is commonly treated as a 40-task classification problem, each task being a binary classification problem for an attribute. As commonly done in previous work (Sener & Koltun, 2018; Yu et al., 2020; Liu et al.,

2021), we employ an encoder-decoder architecture where the encoder is a ResNet-18 (He et al., 2016) (without the final layer), and the per-task decoders are linear classifiers. The cross-entropy loss is used for all tasks. The training is performed from scratch for 50 epochs using Adam, with a mini-batch size of 128 and a per-epoch exponential decay factor of 0.95. As common on this network-dataset combination (Lin et al., 2022; Chen et al., 2020), the initial learning rate is  $\eta = 10^{-3}$  for all methods except for MGDA and IMTL, for which  $\eta = 5 \times 10^{-4}$  yielded a better validation performance. As done by the respective authors, for PCGrad, RLW and GradDrop we use the same learning rate as the unitary scalarization (Yu et al., 2020; Lin et al., 2022; Chen et al., 2020).

#### B.1.3. CITYSCAPES

We rely on the version of the dataset pre-processed by Liu et al. (2019), which consists of 2,975 training and 500 test images and presents two tasks: semantic segmentation on 7 classes, and depth estimation. We further split the original training set into a validation set of 595 images, employed to tune hyper-parameters, and a training set of 2380 images. Consistently with recent work (Lin et al., 2022), we rely on a dilated ResNet-50 architecture pre-trained on ImageNet (Yu et al., 2017) for the encoder, and on the Atrous Spatial Pyramid Pooling (Chen et al., 2018a) as decoders. Cross-entropy loss is employed on the semantic segmentation task, whereas the  $\ell_1$  loss is used for the depth estimation. The training is performed by using Adam with a mini-batch size of 32 for 100 epochs, with an initial step size  $\eta = 5 \times 10^{-4}$  resulting in the best validation performance for all algorithms, exponentially decayed by 0.95 at each epoch.

## B.2. Reinforcement Learning

Similarly to the supervised learning experiments, we ran all the experiments under Ubuntu 18.04 LTS using one GPU per run. Timing experiments were all run using NVIDIA GeForce RTX 2080 Ti GPUs, with an Intel Xeon Gold 6230 CPU. The main bulk of the remaining experiments was run on Nvidia GeForce RTX 2080 Ti GPUs with either Intel Xeon Gold 6230 or Intel Xeon Silver 4216. We utilised NVIDIA GeForce RTX 3080 GPUs with Intel Xeon Gold 6230 CPUs for a small fraction of experiments.

We use Meta-World’s MT10/MT50 for our experiment. The benchmark consists of ten/fifty tasks in which a simulated robot manipulator has to perform various actions, e.g., pressing a button, opening a door, or pushing the block. We use Sodhani et al. (2021) for most of the hyperparameters and list them in Table 1. We use bold font where we use a hyperparameter different from Sodhani et al. (2021). Similarly to Sodhani et al. (2021), we use the v1 version of

Metaworld for our experiments<sup>1</sup>. Sodhani et al. (2021) use a shared entropy loss weight  $\alpha$  for PCGrad and separate  $\alpha$  for unitary scalarization<sup>2</sup>. In our experiments, use shared  $\alpha$  for all of the methods for fairness. Since it is a single number (rather than a vector), we used unitary scalarization to update  $\alpha$  for all SMTOS apart from PCGrad which was already implemented in (Sodhani et al., 2021).

We use the same network architecture as in Sodhani et al. (2021), i.e. a three-layered feedforward fully-connected network with 400 hidden units per layer for both, the actor and the critic. The actor is shared across all tasks as well as the critic.

To normalize rewards, we keep track of first and second moments in the buffer and normalise the rewards by their standard deviation:  $r'_i = r_i/\hat{\sigma}_i$ , where  $\hat{\sigma}_i$  is the sample standard deviation of the rewards for environment  $i$ .

Sodhani et al. (2021) average the gradient for unitary scalarisation and pcgrad, whereas our SMTOS implementations sum the gradients, i.e. effectively using larger learning rates (apart from MGDA that assures that all the aggregation weights sum to 1). We tried reducing the learning rate for SMTOS that sum (RLW Norm., RLW Diri., and GradDrop) both for MT10 and MT50, but it worked worse for these methods and we kept the default learning rate for them as well. We had to use a smaller learning rate for IMTL, because with the default one it crashed at the beginning of training due to numerical overflow. Smaller learning rate did not prevent it from crashing, but this happened much later.

We tried  $10^6$ ,  $2 \times 10^6$ , and  $4 \times 10^6$  for the replay buffer size with the last being superior in terms of stability. Additionally, for  $l_2$  actor regularization, we tried 0.0001 and 0.0003 with the latter being slightly superior for the baseline. We tried the same options for other SMTOS, and picked the best option for each of the method. For MGDA, no regularisation works best, most likely due to a strong regularization effect of the method itself, which is mirrored by our supervised learning results. PCGrad and Graddrop work best with the regularization coefficient of 0.0001. Both RLW variants use the same coefficient as the baseline (0.0003).

For MT50, we took the best MT10 hyperparameters, and we believe one could obtain even better results for unitary scalarisation since it is much faster to tune compared to other SMTOS (e.g. 15 hours for unitary scalarisation vs 9 days for PCGrad).

<sup>1</sup><https://github.com/rlworkgroup/metaworld.git@af8417bfc82a3e249b4b02156518d775f29eb289>

<sup>2</sup><https://mtrl.readthedocs.io/en/latest/pages/tutorials/baseline.html>

Table 1. Hyperparameters of the RL experiments. Hyperparameters different from Sodhani et al. (2021) are in bold.

Hyperparameter	Value
All methods	
– training steps	2,000,000
– batch size	1280
– <b>Replay buffer size</b>	<b>4,000,000</b>
– actor learning rate	0.0003
– critic learning rate	0.0003
– entropy $\alpha$ learning rate	0.0003
– shared entropy $\alpha$	True
– runs	10
– discounting $\gamma$	0.99
Unit. Scal.	
– <b>actor <math>l_2</math> coeff.</b>	<b>0.0003</b>
PCGrad	
– <b>actor <math>l_2</math> coeff.</b>	<b>0.0001</b>
RLW Norm.	
– normal mean	0
– normal std	1
– actor $l_2$ coeff.	0.0003
RLW Diri.	
– $\alpha$	1
– actor $l_2$ coeff.	0.0003
GradDrop	
– k	1
– p	0.5
– actor $l_2$ coeff.	0.0001
MGDA	
– gradient normalization	$L_2$
– actor $l_2$ coeff.	0.0
IMTL	
– actor learning rate	0.00003
– critic learning rate	0.00003
– entropy $\alpha$ learning rate	0.00003
– actor $l_2$ coeff.	0.0

## C. Supplementary Supervised Learning Experiments

This section presents supervised learning results omitted from §5.1. In particular, we show additional plots for the experiments of §5.1, then present an analysis of the regularising effect of SMTOS in the absence of single-task regularization (§C.2), and conclude with an ablation study on GradDrop’s dependency on the sign of per-task gradi-

ents (§C.3).

## C.1. Addendum

This section complements the plots presented in §5.1. In particular, we show the test and runtime results in table form, along with the behavior of the validation metrics and of the training loss over the training epochs. Plots for Multi-MNIST, CelebA, and Cityscapes are reported in Figures 7, 8 and 14, respectively. The Multi-MNIST plots show that all optimizers are relatively stable and drive each task’s loss towards its global minimum of 0. The behavior of the CelebA training loss demonstrates heavier regularization (compare with the unregularized plot in Figure 9(a)). Except IMTL and MGDA, for which the tuned values of the weight decay prevent overfitting, the other optimizers display very similar validation and training curves, and start overfitting around epoch 30. Considering that most SMTOS required less regularization (see §5.1.2), the results are consistent with our interpretation of SMTOS as regularizers in §4. The Cityscapes plots display a certain instability across training epochs, as demonstrated by the various peaks and valleys in the metrics. Nevertheless, in spite of a factor 10 difference in scale, both training losses are rapidly driven towards 0 by most optimizers.

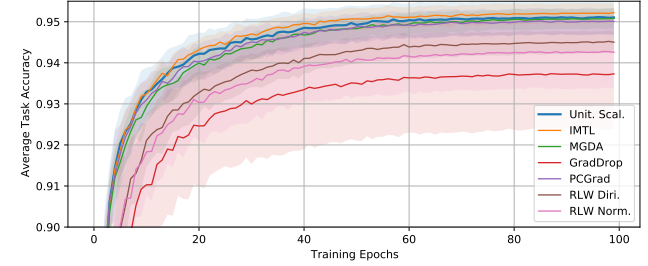
## C.2. Unregularized Experiments

In Section 4, we interpret SMTOS through the lens of regularization. In order to provide an empirical assessment of the technical results presented in §4, we repeat the CelebA (Liu et al., 2015) results from §5.1.2 and remove any form of regularization. In other words, no dropout layers are added to the encoder-decoder architecture, and  $\lambda = 0$  ( $\ell_2$  regularization) for all optimizers. In addition, we plot the behavior of two different  $\ell_2$ -regularized instances of unitary scalarization:  $\lambda = 10^{-4}$  for the curve named “Unit. Scal.  $\ell_2$ ”,  $\lambda = 2 \times 10^{-3}$  for the curve named “Unit. Scal.  $\ell_2+$ ”. Furthermore, “Unit. Scal. Reg.” plots the regularized unitary scalarization from §5.1.2, which uses both dropout layers and a weight decay of  $\lambda = 10^{-3}$ .

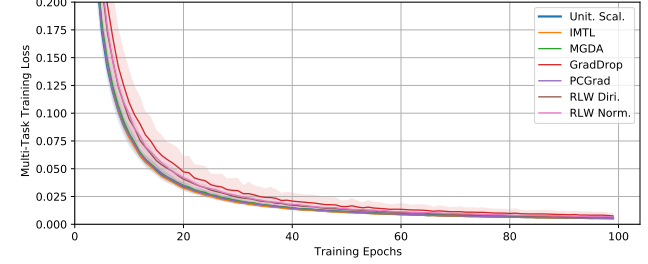
Figures 1, 9(a) and 9(b) respectively report the average task validation accuracy, the multi-task training loss, and the multi-task validation loss at each training epoch. The regularizing effect of SMTOS compared to unitary scalarization is shown by: (i) the delay of the onset of overfitting on the validation data in figure 1, (ii) the reduction of the convergence rate on the training loss in figure 9(a) (compare with figure 8(c)), and (iii) the fact that validation and training losses remain positively correlated for larger numbers of epochs. In fact, the behavior of both the training and validation loss for the SMTOS closely parallels that of  $\ell_2$ -regularized unitary scalarization, with differing degrees of regularization. We further note that unregularized IMTL

(a) Mean and 95% CI of the avg. task test accuracy across runs, and interquartile range for the training time per epoch.

MTO	Average Task Accuracy	Epoch Runtime [s]
Unit. Scal.	$9.476e-01 \pm 4.368e-03$	$[3.510e+00, 3.617e+00]$
IMTL	$9.487e-01 \pm 2.533e-03$	$[3.695e+00, 3.996e+00]$
MGDA	$9.478e-01 \pm 1.977e-03$	$[3.491e+00, 3.617e+00]$
GradDrop	$9.347e-01 \pm 1.282e-02$	$[3.508e+00, 3.589e+00]$
PCGrad	$9.479e-01 \pm 3.578e-03$	$[3.807e+00, 3.928e+00]$
RLW Diri.	$9.430e-01 \pm 2.973e-03$	$[3.790e+00, 4.005e+00]$
RLW Norm.	$9.399e-01 \pm 8.929e-03$	$[3.894e+00, 4.225e+00]$



(b) Mean (and 95% CI) average task validation accuracy per training epoch.



(c) Mean (and 95% CI) training multi-task loss  $\mathcal{L}^{\text{MT}}$  per epoch.

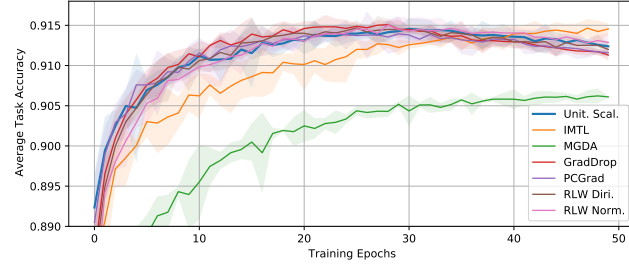
Figure 7. Additional figures for the comparison of various SMTOS with the unitary scalarization on the MultiMNIST dataset (Sener & Koltun, 2018).

displays a certain instability (compare with the regularized version in figure 8(b)).

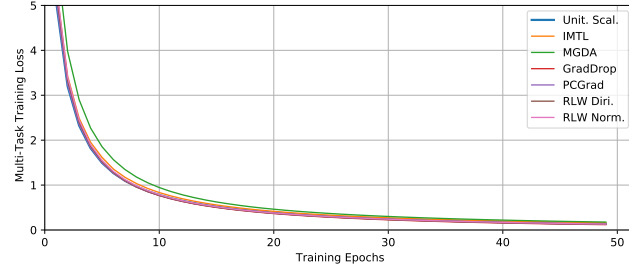
The addition of dropout layers further reduces overfitting, improves stability (reduced confidence intervals) and pushes the average validation curve upwards, motivating its use on all optimizers for the experiments of §5.1.2. Nevertheless, confidence intervals in Figure 1 still overlap due to the instability of the unregularized unitary scalarization. Figure 10 provides a more detailed comparison over 20 repetitions, confirming that the combined use of dropout layers and  $\ell_2$  regularization improves average performance and reduces the empirical variance for unitary scalarization. We conclude by pointing out that even without regularization, when carefully tuned, the maximal performance over epochs of unitary scalarization is comparable to SMTOS in Figure 1.

(a) Mean and 95% CI of the avg. task test accuracy across runs, and interquartile range for the training time per epoch.

MTO	Average Task Accuracy	Epoch Runtime [s]
Unit. Scal.	$9.090e-01 \pm 7.568e-04$	[ $2.869e+02, 2.878e+02$ ]
IMTL	$9.093e-01 \pm 7.631e-04$	[ $3.600e+02, 3.621e+02$ ]
MGDA	$9.022e-01 \pm 9.687e-04$	[ $6.859e+02, 7.194e+02$ ]
GradDrop	$9.098e-01 \pm 3.383e-04$	[ $3.001e+02, 3.008e+02$ ]
PCGrad	$9.093e-01 \pm 1.108e-03$	[ $1.015e+04, 1.016e+04$ ]
RLW Diri.	$9.099e-01 \pm 7.845e-04$	[ $3.040e+02, 3.054e+02$ ]
RLW Norm.	$9.095e-01 \pm 1.012e-03$	[ $3.028e+02, 3.037e+02$ ]



(b) Mean (and 95% CI) average task validation accuracy per training epoch.



(c) Mean (and 95% CI) training multi-task loss  $\mathcal{L}^{\text{MT}}$  per epoch.

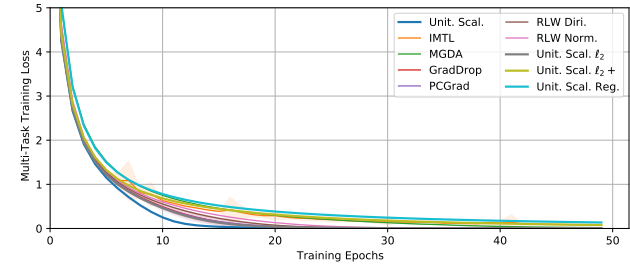
Figure 8. Additional figures for the comparison of various SMTOs with the unitary scalarization on the CelebA (Liu et al., 2015) dataset.

### C.3. Sign-Agnostic GradDrop

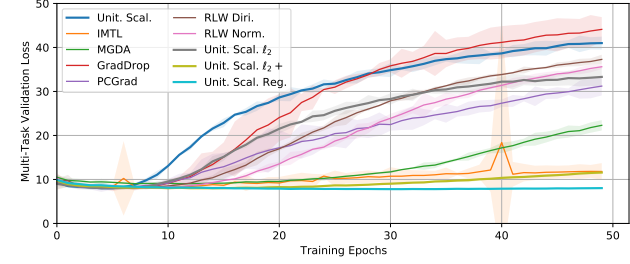
We will now present an ablation study on GradDrop, investigating the effect of the sign of per-task gradients on the SMTO’s performance. Specifically, we compare the performance of GradDrop with a sign-agnostic version of its stochastic gradient masking (which we refer to as “Sign-Agnostic GradDrop”), whose update direction is defined as follows:

$$\mathbf{g} = - \left( \frac{\partial \mathbf{z}}{\partial \theta_{\parallel}} \right)^T \left( \sum_{i \in \mathcal{T}} \mathbf{u}_i \odot \nabla_{\mathbf{z}} \mathcal{L}_i \right),$$

where  $\mathbf{u}_i, \nabla_{\mathbf{z}} \mathcal{L}_i \in \mathbb{R}^{n \times r}$  and, for all  $i \in \mathcal{T}$ ,  $\mathbf{u}_i$  is i.i.d. according to  $\mathbf{u}_i[j, k] \sim \text{Bernoulli}(p) \forall j \in \{1, \dots, n\}, k \in \{1, \dots, r\}$ . Differently from a similar study carried out by Chen et al. (2020), we tuned the hyper-parameter of the sign-agnostic masking in the following range:  $p \in \{0.1, 0.25, 0.5, 0.75, 0.9\}$ .



(a) Mean and 95% CI (3 runs) multi-task training loss per epoch.



(b) Mean and 95% CI (3 runs) multi-task validation loss per training epoch.

Figure 9. Additional figures for the unregularized comparison of various SMTOs with the unitary scalarization on CelebA. SMTOs provide varying degrees of regularization.

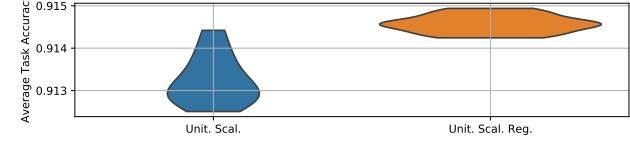


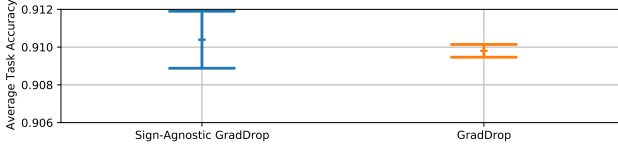
Figure 10. Effect of regularization (dropout layers and weight decay) on unitary scalarization on the CelebA dataset: violin plots (20 runs) for the best avg. task validation accuracy over epochs. The width at a given value represents the proportion of runs yielding that result. Regularization improves the average performance while decreasing its variability.

The experimental setup complies with the one described in appendix B.1. Figure 11, plotting test and validation results for the CelebA dataset (Liu et al., 2015), shows that the performance of Sign-Agnostic GradDrop closely matches the original algorithm. Therefore, sign conflicts across per-task gradients do not seem to play a significant role in GradDrop’s performance.

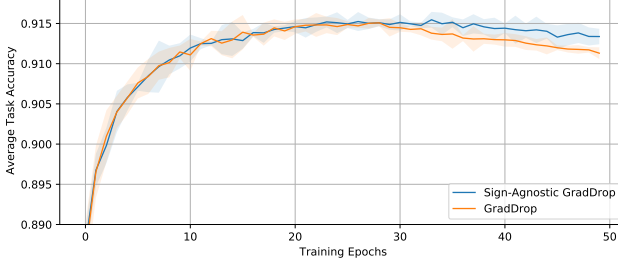
## D. Supplementary Reinforcement Learning Experiments

### D.1. Ablation studies

Figure 15 presents our ablations for MT10 experiments. Due to computational constraints, we ran ablations on the unitary scalarization and PCGrad since these are the two methods previously tested in the RL setting.

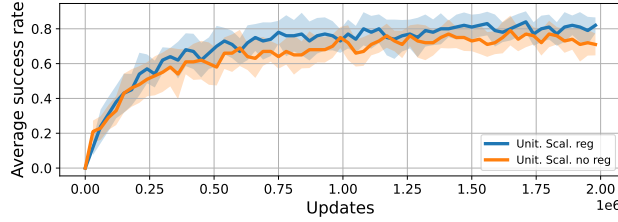


(a) Mean and 95% CI (3 runs) avg. task test accuracy.

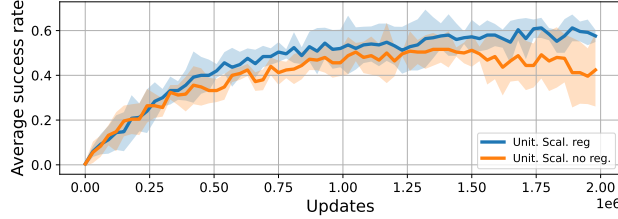


(b) Mean and 95% CI (3 runs) avg. task validation accuracy per training epoch.

Figure 11. Comparison of GradDrop (Chen et al., 2020) with sign-agnostic masking of the shared-representation gradients on the CelebA dataset (Liu et al., 2015). No statistically relevant difference between the two methods can be observed for the majority of the epochs.



(a) MT10 average performance (10 runs) and 95% CI.



(b) MT50 average performance (5 runs) and 95% CI.

Figure 12. For both MT10 and MT50, actor  $l_2$  regularization pushes the average higher for unitary scalarization.

Figure 12 shows ablation studies on the effect of regularization on MT10 and MT50. In spite of CI overlaps, actor  $l_2$  regularization pushes the average higher on both benchmarks, motivating our use of regularization for the experiments in §5.2. Furthermore, the gap between the averages tends to widen with the number of updates on MT50, suggesting improved stabilization.

## D.2. Sensitivity to Reward Normalization

Figure 13 shows that multitask agent performance is highly sensitive to the reward normalization moving average hyperparameter<sup>3</sup> motivating our buffer normalization in Section 5.2.

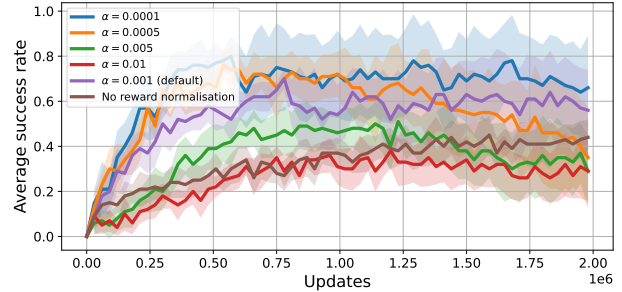
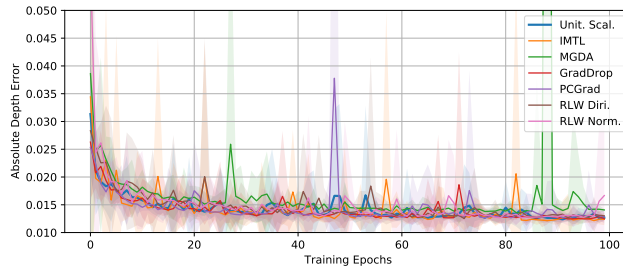


Figure 13. The learning outcomes of a Multitask SAC agent vary considerably depending on the reward normalisation hyperparameter. Each of the curves represents and average of 10 runs with shaded 95% confidence interval.

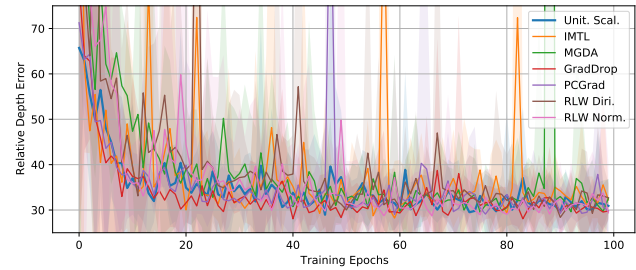
<sup>3</sup>[https://github.com/facebookresearch/mtenv/blob/4a6d9d6fdfb321f1b51f890ef36b5161359e972d/mtenv/envs/metaworld/wrappers/normalized\\_env.py#L69](https://github.com/facebookresearch/mtenv/blob/4a6d9d6fdfb321f1b51f890ef36b5161359e972d/mtenv/envs/metaworld/wrappers/normalized_env.py#L69)

(a) Mean and 95% CI of the test metrics across runs, and interquartile range for the training time per epoch.

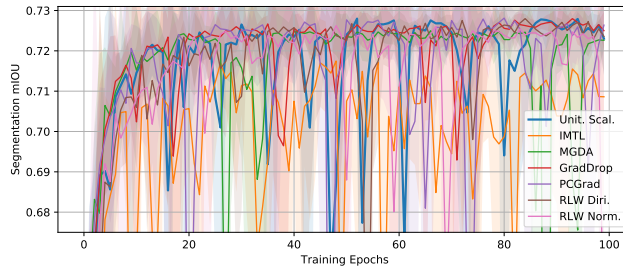
MTO	Absolute Depth Error	Relative Depth Error	Segmentation Accuracy	Segmentation mIOU	Epoch Runtime [s]
Unit. Scal.	1.301e-02 $\pm$ 2.342e-04	4.761e+01 $\pm$ 5.148e+00	9.196e-01 $\pm$ 2.913e-04	7.012e-01 $\pm$ 6.001e-04	[3.228e+02, 3.241e+02]
IMTL	1.281e-02 $\pm$ 7.521e-04	4.389e+01 $\pm$ 6.984e-01	9.164e-01 $\pm$ 2.828e-03	6.967e-01 $\pm$ 4.785e-03	[7.329e+02, 7.373e+02]
MGDA	1.418e-02 $\pm$ 2.331e-04	4.750e+01 $\pm$ 1.466e+01	9.189e-01 $\pm$ 2.636e-04	6.999e-01 $\pm$ 3.124e-03	[7.251e+02, 7.269e+02]
GradDrop	1.293e-02 $\pm$ 2.757e-04	4.674e+01 $\pm$ 7.709e+00	9.193e-01 $\pm$ 1.282e-03	7.024e-01 $\pm$ 3.628e-03	[5.196e+02, 5.215e+02]
PCGrad	1.294e-02 $\pm$ 2.284e-04	4.380e+01 $\pm$ 5.165e+00	9.198e-01 $\pm$ 9.119e-04	7.025e-01 $\pm$ 6.531e-04	[4.202e+02, 4.212e+02]
RLW Diri.	1.305e-02 $\pm$ 4.155e-04	4.810e+01 $\pm$ 2.259e+00	9.199e-01 $\pm$ 1.247e-03	7.037e-01 $\pm$ 1.989e-03	[3.161e+02, 3.164e+02]
RLW Norm.	1.301e-02 $\pm$ 5.528e-04	4.630e+01 $\pm$ 2.751e+00	9.192e-01 $\pm$ 4.962e-04	7.006e-01 $\pm$ 4.580e-03	[3.194e+02, 3.210e+02]



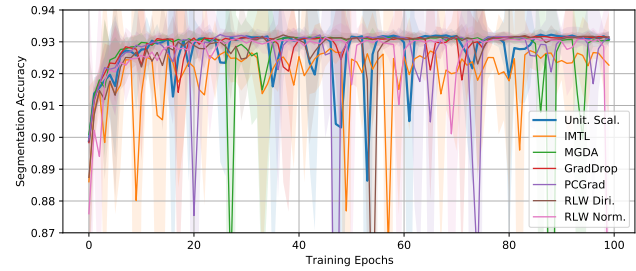
(b) Mean (and 95% CI) absolute depth validation error per training epoch.



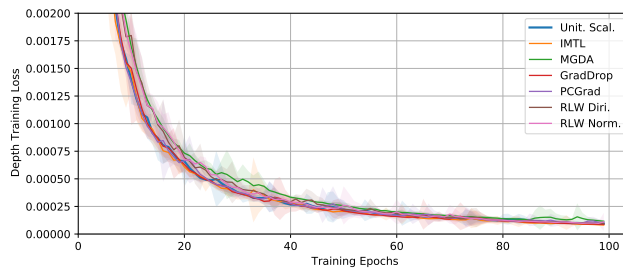
(c) Mean (and 95% CI) relative depth validation error per training epoch.



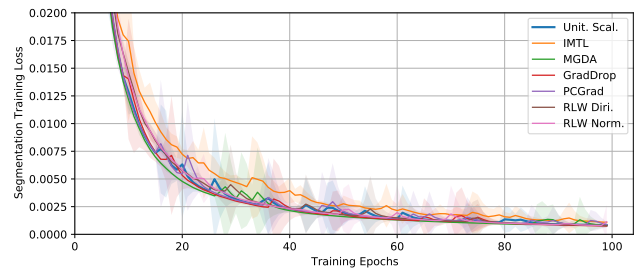
(d) Mean (and 95% CI) validation segmentation mIOU per training epoch.



(e) Mean (and 95% CI) validation segmentation accuracy per training epoch.



(f) Mean (and 95% CI) training depth loss per epoch.

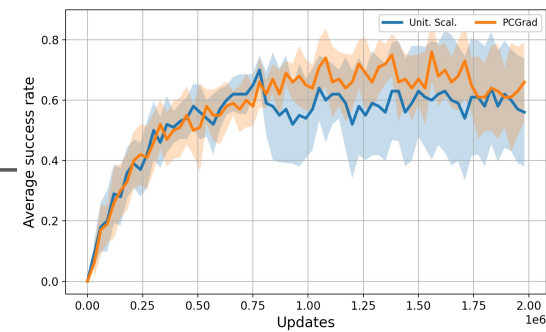
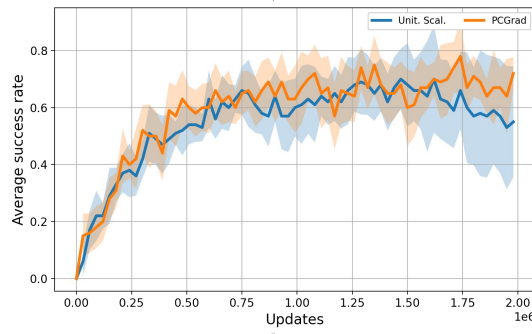


(g) Mean (and 95% CI) training segmentation loss per epoch.

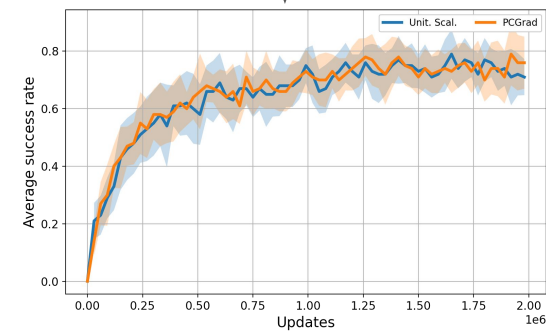
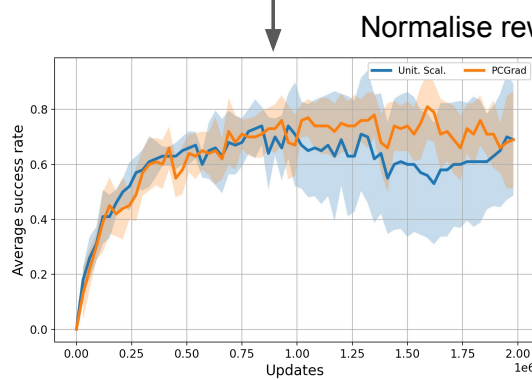
Figure 14. Additional figures for the comparison of SMTOS with the unitary scalarization on the Cityscapes (Cordts et al., 2016) dataset.

## Hyperparameters from [Sodhani et al, 2021]

Use PCGrad parameters for the baseline (shared alpha)



Increase replay buffer size



Normalise reward at the buffer level

Regularize the actor

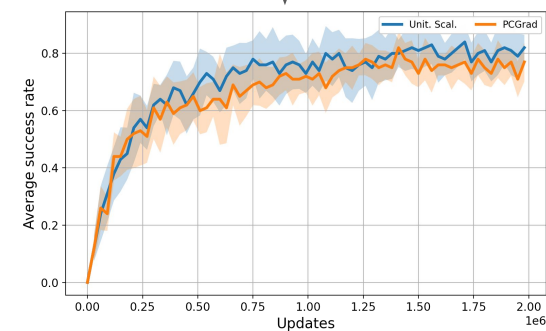


Figure 15. Metaworld's MT10 ablation experiments.